

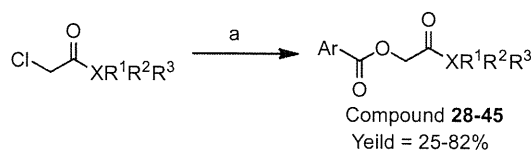
a hydrophobic substitute. The nitro-furan ring is connected to the amide group through an ester linkage. Synthesis of these chemicals was accomplished by coupling reaction of nitro-furoic acid with α -chloro carbonylate containing of a hydrophobic substitute and an amide group. Hence, three series of analogue compounds were synthesized by the following strategy for modulating parts A, B and C of Figure 1a: (A) conversion of the hydrophobic substitute bound to the amide group to other substitutes, (B) conversion of the nitro-furan ring to several other chemical structures, and (C) conversion of the ester linkage to an amide bond.

The 50% inhibitory concentration (IC_{50}) of the compounds for HIV-1 RT-associated RNase H activity was determined from the chemical concentration leading half the rate for substrate cleavage reaction relative to the control. A real-time monitoring assay was carried out to estimate IC_{50} of the synthesized compounds.

As shown in Table 1 and 28 analogues were synthesized by converting the hydrophobic substitute at part A. In the in vitro assay for inhibitory activity, most of the analogues exhibited a similar degree of inhibitory potency to the hit chemical in Figure 1a, the IC_{50} value of which was 16.5 μ M. Inhibitory activity was retained with conversion of the amide bond to an ester linkage and substitution of the hydrophobic region with *iso*-propyl (**1**). A set of derivatives containing two methyl groups and one hydrophobic substitute such as *t*-butyl, pentyl or phenyl bound to an alkyl carbon connecting to the amide group was surveyed (**2–5**). Substitution of tetrahydrofuran was also tested (**6**). These derivatives had similar potencies. In particular, tetrahydrofuran substitution (**6**) increased compound potency by approximately fourfold from the hit chemical. The effect of introduction of a phenyl group was examined in two forms: one is through connection with cyclo-carbons

Table 2

Structure and RNase H inhibitory activity of the derivatives modulated at part B



Conditions ; (a) Ar-CO₂H, DMAP, DMF, 80 °C, 6 h

Compound	X	Ar-CO ₂ H	R ¹ , R ² , R ³	Yield (%)	IC ₅₀ (μ M)
29	N	<i>o</i> -Nitro-C ₆ H ₄ CO ₂ H	R ¹ = H, R ² = <i>t</i> -Bu	57	>50
30		<i>m</i> -Nitro-C ₆ H ₄ CO ₂ H	R ¹ = H, R ² = <i>t</i> -Bu	60	>50
31		<i>p</i> -Nitro-C ₆ H ₄ CO ₂ H	R ¹ = H, R ² = <i>t</i> -Bu	49	>50
32		3,5-Dinitro-C ₆ H ₃ CO ₂ H	R ¹ = <i>t</i> -Bu, R ² = CH ₂ Ph	34	>50
33	N		R ¹ = <i>t</i> -Bu, R ² = CH ₂ Ph	67	>50
34			R ¹ = H, R ² = <i>t</i> -Bu	30	>50
35	N		R ¹ = H, R ² = <i>t</i> -Bu	43	>50
36			R ¹ = H, R ² = <i>t</i> -Bu	25	>50
37			R ¹ = H, R ² = <i>t</i> -Bu	82	>50
38	N		R ¹ = H, R ² = <i>t</i> -Bu	61	>50
39			R ¹ = H, R ² = <i>t</i> -Bu	46	>50
40			R ¹ = H, R ² = <i>t</i> -Bu	61	2.8
41	N		R ¹ = H, R ² = CMe ₂ Et	32	5.8
42			R ¹ = CMe ₂ Et, R ² = CH ₂ <i>p</i> -NO ₂ C ₆ H ₄	58	33.5
43			R ¹ = CMe ₂ Et, R ² = CH ₂ <i>m</i> -NO ₂ C ₆ H ₄	64	25.8
44	C		R ¹ = H, R ² = H, R ³ = H	56	9.5
45			R ¹ = Me, R ² = Me, R ³ = Me	48	5.7

Conditions: (a) Ar-CO₂H, DMAP, DMF, 80 °C, 6 h.

(7–9) and the other with an alkyl chain (10–13). A highly potent compound (10) was found in the analogues in which a benzyl group with a *t*-butyl substitute was introduced. This derivative (10) showed an 18-fold increment of RNase H inhibitory activity from the original hit chemical. In contrast, no inhibitory activity was observed for the analogues with a phenyl group introduced via more than two chain atoms of carbon or oxygen (12 and 13). The effect of introduction of a phenyl group via an alkyl chain was further examined by connecting some polar functional groups, nitro, acetyl, methoxy and phenoxy, to the phenyl (14–19). These derivatives showed inhibitory activities similar to that of the hit chemical, while no activity was observed only for the connection of phenoxy (19), which was a considerably large substitute. The introduction of fluoride was examined with the phenyl group linked to an amide bond via an alkyl chain (20–24). These derivatives exhibited similar degrees of inhibitory activity, but no highly potent compound was found with fluoride introduction. The introduction of tetrahydrofuran with a benzyl or hydroxy benzyl group (25 and 26) was examined. Both compounds showed inhibitory activity similar to that of the hit chemical. The amide group was converted to a carbonyl group (27 and 28). A similar degree of inhibitory activity was maintained with conversion of the amide bond to an acetyl group, while conversion to oxy *t*-butyl decreased the inhibitory potency.

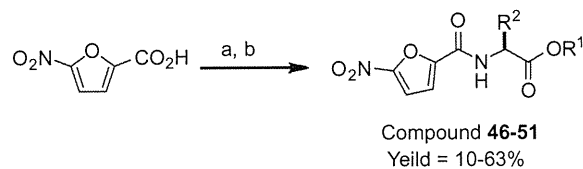
As shown in Table 2 and 17 analogues were synthesized by converting the nitro-furan ring at part B into other ring structures. Most of the analogues lost inhibitory potency for RNase H enzymatic activity or had significantly reduced inhibitory activity. Conversion of the furan ring into benzene (29–32) resulted in loss of compound potency, regardless of the location of the nitro group at the *ortho*-, *meta*- or *para*-position. The derivative containing two nitro groups (32) also showed no inhibitory activity. A series of derivatives with modification of the nitro group (33–36) exhibited no inhibitory activity. Removal of the nitro group (33), replacement by bromide (34), replacement by carbonyl phenyl (35), or removal of even hydrogen (36) resulted in complete loss of compound potency. Substitution of the nitro group by nitro-benzene (37–39) resulted in no inhibitory activity regardless of the position of the nitro group bonding to benzene. Substitution of the furan ring with thiophene (40–45) was surveyed. Some derivatives were more potent than the hit chemical. An analog derived from compound 3 with conversion of the furan ring into thiophene (40) showed high inhibitory activity.

As shown in Table 3 and six analogues were synthesized by exchanging the ester bond at part C. Ester linkage is disadvantageous for medicine because esterase digests the linkage and the drug concentration in a body is rapidly decreased. The ester linkage was replaced by an amide group (46–51). None of the derivatives showed noticeable inhibitory activity.

As shown in Table 4 and two analogues were synthesized by converting the region connected to the ester bond at parts A and C. Both derivatives (52 and 53) increased compound potency 6–8-fold from the hit chemical. It is interesting to note that the distance from the ring part of the substituted moiety to the ester bond is small compared to a series of derivatives listed in Table 1.

In the measurement of cytotoxicity using MT-4 cells, almost all chemical compounds showed no cytotoxicity at a concentration of 100 μ M, except for compounds 21, 23, 52 and 53 as shown in Table 5. In the measurement using 293T cells, many compounds showed no noticeable cytotoxicity at a concentration of 100 μ M, while seven compounds, 11, 15, 21, 22, 23, 24 and 52 showed cytotoxicity in which CC_{50} ranged from 36 to 83 μ M. Compounds showing cytotoxicity contain several fluoride atoms (21–24). Cytotoxicity was also observed in a compound bearing a nitro-benzyl group (15 and 52), which is a chemical structure known as a cause for genotoxicity. Overall, the assessment of cytotoxicity suggested

Table 3
Structure and RNase H inhibitory activity of the derivatives modulated at part C



Conditions : (a) $SOCl_2$, CH_2Cl_2 , reflux, 3 h,
(b) Aminoacidester, NEt_3 , CH_2Cl_2 , 0 °C-rt, 1 h

Compound	R ¹ , R ²	Yield (%)	IC ₅₀ (μ M)
46	R ¹ = Me, R ² = H	10	>50
47	R ¹ = Et, R ² = Me	70	>50
48	R ¹ = Et, R ² = CH_2i -Pr	45	>50
49	R ¹ = Et, R ² = CH_2 Ph	60	>50
50	R ¹ = Et, R ² = CH_2p -OHC ₆ H ₄	63	>50
51	R ¹ = Et, R ² = Ph	61	>50

Conditions: (a) $SOCl_2$, CH_2Cl_2 , reflux, 3 h; (b) amino acid ester, NEt_3 , CH_2Cl_2 , 0 °C to rt, 1 h.

that a nitro-furan core has little cytotoxicity for MT-4 and 293T cells and that the scaffold tested in this study is favorable from a cytotoxic viewpoint. It is notable that there is some degree of difference in concentrations of compounds showing noticeable cytotoxicity between MT-4 and 293T cells.

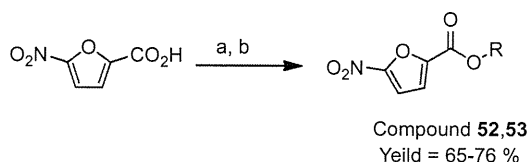
4. Discussion

Two hit chemicals found in our previous in vitro screening bear an ester linkage at the connection of the nitro-furan group and the hydrophobic moiety.¹⁷ All of the compounds showing RNase H inhibitory activity in Tables 1 and 2 have this ester linkage. Table 3 clearly indicates that conversion of the ester linkage into an amide bond results in loss of inhibitory potency. The amide bond is likely to form a planar configuration. Hence, a straight form is favorable for the amide linkage of nitro-furan and the hydrophobic moiety. If a compound has a straight form, the side part of the compound will collide with the inside wall of the binding pocket of the RNase H domain. Accordingly, it will be difficult for the compound to combine with the binding pocket. This suggests that an amide bond adjacent to the nitro-furan group is unfavorable for RNase H inhibitors.

As shown in Table 1, no drastic change was observed in inhibitory activity when the hydrophobic moiety connecting to carbonyl carbon was substituted by various kinds of chemical groups. This indicates that the substituted region has little interaction with the RNase H domain, suggesting that the substituted region will be located outside the binding pocket and exposed to the solvent. This indicates that a strategy for increasing inhibitory activity is for the position of the substitute to be closer to the nitro-furan group or instead more distant from it. The former conversion may make the aromatic ring or hydrophobic substitute interact with the target protein inside the binding pocket. The latter will make the substitute interact with a neighboring hollow site outside the binding pocket.

Table 2 shows that conversion of the nitro-furan group into other chemical structures drastically decreases the inhibitory activity except for nitro-thiophene. This means that a nitro-furan core is indispensable for inhibitory potency induced by analogues of the hit chemical in Figure 1a. The characteristic property of nitro-furan is large electric polarity. Oxygen atoms are negatively charged. These oxygen atoms will be coordinated to divalent metal ions at the RNase H active site. Accordingly, enhancing the

Table 4
Structure and RNase H inhibitory activity of the derivatives modulated at the moiety connected to the ester bond in parts A and C



Conditions ; (a) SOCl_2 , CH_2Cl_2 , reflux, 3 h,
(b) Nucleophile, NEt_3 , CH_2Cl_2 , 0 °C-rt, 1 h

Compound	Nucleophile	R	Yield (%)	IC ₅₀ (μM)
52		R = $(\text{CH}_2)_2p\text{-NO}_2\text{C}_6\text{H}_4$	76	2.1
53		R =	65	2.7

Conditions: (a) SOCl_2 , CH_2Cl_2 , reflux, 3 h; (b) nucleophile, NEt_3 , OH_2O_2 , 0 °C to rt, 1 h.

Table 5
Evaluation of cytotoxicity of the synthesized compounds

Compound	CC ₅₀ (μM): MT-4	CC ₅₀ (μM): 293T	Compound	CC ₅₀ (μM): MT-4	CC ₅₀ (μM): 293T
1	>100	>100	29	—	—
2	>100	>100	30	—	—
3	>100	>100	31	—	—
4	>100	>100	32	—	—
5	>100	>100	33	—	—
6	>100	>100	34	—	—
7	>100	>100	35	—	—
8	>100	>100	36	—	—
9	>100	>100	37	—	—
10	>100	>100	38	—	—
11	>100	67	39	—	—
12	—	—	40	>100	>100
13	—	—	41	—	—
14	>100	>100	42	—	—
15	>100	78	43	—	—
16	>100	>100	44	—	—
17	>100	>100	45	—	—
18	>100	>100			
19	—	—	46	—	—
20	>100	>100	47	—	—
21	71	36	48	—	—
22	>100	68	49	—	—
23	95	65	50	—	—
24	>100	83	51	—	—
25	>100	>100	52	28	36
26	>100	>100	53	86	>100
27	>100	>100			
28	>100	>100			

— means that the measurement for cytotoxicity was not performed because the compound shows no or little inhibitory activity.

coordination force to metal ions is one strategy for increasing inhibitory activity.

RNase H of HIV-1 exerts its enzymatic activity by incorporating divalent metal ions at the reaction site.^{26,27} In April 2009, there were 119 entries for the crystal structure of HIV-1 reverse transcriptase in Protein Data Bank. We surveyed the number of divalent metal ions observed at the RNase H domain through all of these 119 crystal structures. As shown in Table S1 in Supplementary data, no metal ion was observed in many of the crystal structures. The presence of Mg^{2+} ions was detected in 16 crystal structures and coordination of Mn^{2+} ions was observed in five structures. Mn^{2+} ion is often used in protein crystallization, because the

coordination force to the active site becomes strong with change from Mg and Mn. A single metal ion is observed in most metal-bound crystal structures. Double coordination of divalent metal ions was observed only in 1RTD²⁸ at that time point. Accordingly, it had been controversial how many metal ions were required at the RNase H reaction site to exert its enzymatic activity.^{18,29} A theoretical study by De Vivo et al. suggested that the presence of two divalent metal ions is essential for RNase H activity and that two metal ions act cooperatively with facilitating nucleophilic binding of a substrate and stabilizing the transition state for the enzymatic reaction.³⁰ De Vivo et al. also suggested that there is a difference in role of those two metal ions. One of the ions is stably bound to the

RNase H active site with an ideal octahedral coordination through the reaction, while the other is slightly irregular with changing the coordination bond. This theoretical finding strongly suggests double coordination of divalent metal ions at the RNase H domain, but the number of coordinated metal ions was still not clearly determined when an RNase H inhibitor was bound to the active site.

From the latter half of 2009, crystal structures on the complex of the RNase H domain and its inhibitor were successively reported from three different research groups.^{6–8} All of the crystal structures in the reports showed the presence of two metal ions at the active site. One of the divalent metal ions was held deep inside the binding pocket of the RT RNase H domain with making coordination bonds to three carboxyl groups of Asp443, Glu478 and Asp498. The other was fixed with making coordination bonds to two carboxyl groups of Asp443 and Asp549. The distance between two metal ions was about 4 Å. Every inhibitor in crystal structures was revealed to have a similar binding mode. That is, inhibitors are stabilized with forming coordination bonds to both metal ions.

In the X-ray crystallographic study by Kirschberg et al.⁶ the crystallization was achieved using the isolated RNase H domain. The inhibitor was a kind of pyrimidinol carboxylic acid derivative. This compound bears a pyrimidine ring connected to one carboxyl group and two hydroxyl groups. This chemical structure shows a significant feature of negatively charged functional groups being aligned in a straight form. This negatively charged region is strongly attached to two divalent metal ions. An oxygen atom located at the center of the straightly aligned polar atoms is positioned between the two metal ions. In their study, many chemical structures were examined by modulating the substitute located at the position opposite the straightly aligned negatively charged atoms on the pyrimidine ring. IC₅₀ values of the derivatives were ranged from 0.1 to 70 μM. In their crystal structure; PDB code: 3HYF, the inhibitor has a dichlorobenzyl group as a substitute at the opposite region on the pyrimidine ring. This region was demonstrated to stick out from the binding pocket and to be exposed to the solvent.

An X-ray crystallographic study by Himmel et al.⁷ was performed using a protein expressed by RT69A vector. The protein consists of the RT p66 subunit containing F160S and C280S mutations and the p51 subunit containing C280S mutation and truncated at residue 428. The *apo*-crystal without an inhibitor using this protein was reported to give a high-resolution X-ray diffraction.²⁰ The X-ray analysis by Himmel et al. is the first report for co-crystallization of whole RT and an RNase H inhibitor. The inhibitor was β-thujaplicinol, which shows a high level of RNase H inhibitory activity.¹⁶ β-Thujaplicinol has a unique chemical structure, in which two hydroxyl groups and one carbonyl group are connected to the adjacent three carbon atoms on a seven-member ring. Those negatively charged oxygen atoms are also aligned in a straight form in a manner similar to that for pyrimidinol carboxylic acids. These negatively charged atoms are strongly coordinated to two divalent metal ions. All of the charged atoms are located on one side of the seven-member ring and the oxygen atom positioned at the center of the three aligned negatively charged atoms is coordinated to both metal ions. An alkyl chain is connected to the region opposite to the three negatively charged atoms on the seven-member ring in β-thujaplicinol. In the X-ray crystal structure; PDB code: 3IG1, this alkyl chain was demonstrated to be located outside the binding pocket and exposed to the solvent.

Su et al. also provided X-ray crystal structures on the complex of full-length HIV-1 RT and chemical compounds showing RNase H inhibitory activity.⁸ The chemical compounds have a structural basis of pyridine hetero-rings to which one hydroxyl group and one carbonyl group are connected. IC₅₀ values of those pyridine heteroring-based derivatives were reported to be 0.1–0.2 μM. The chemical structure also shows a common feature of negatively

charged atoms being aligned in a straight form. This negatively charged region was strongly bound to two divalent metal ions. The oxygen atom located at the center of the straightly aligned polar atoms was positioned between the two metal ions. Ethoxy or cyclo-pentane groups are attached to the side opposite the negatively charged region on the hetero-rings. These groups were also shown to stick out from the binding pocket and to be exposed to the solvent in the crystal structures; PDB codes: 3LP0 and 3LP1.

The above three X-ray crystal analyses have revealed that the RNase H active site holds two divalent metal ions and that an RNase H inhibitor is bound to the active site with forming coordination bonds to these metal ions. Accordingly, it is highly probable that the chemical compounds showing RNase H inhibitory activity examined in this study are also coordinated to two divalent metal ions. These compounds have a structural core of nitro-furan and bear an ester linkage at the site opposite the nitro group on the furan ring. Hence, negatively charged oxygen atoms of the nitro group, furan, and carbonyl group are aligned in a straight form. This negatively charged region will be attached to the divalent metal ions.

In order to examine whether the binding mode described in the above paragraph is stable or not, theoretical calculation with QM/MM method was performed. Geometry of the QM region was optimized in the B3LYP/6-31G(d,p) level and that for the MM region was optimized by molecular mechanics approach with the universal force field. All of the atoms were allowed to move freely during geometry optimization. The X-ray crystal structure; PDB code: 3HYF,⁶ was used for the computational model for the RNase H domain. The initial atom coordinates before geometry optimization were set to the same as those of the crystal structure. The inhibitor, two Mg²⁺ ions, and side chains of Asp443, Glu478, Asp498, Asp549 and His 539 were assigned to the atoms in the QM region. QM/MM calculations were executed using three kinds of chemical compounds; **3**, **7** and **10**. The dashed lines in Table 1 separate the compounds into several groups in terms of chemical structure, and compounds; **3**, **7** and **10**, bear a typical chemical structure of each group. The inhibitory activity of these compounds is high and the mass-weight is relatively low compared to other chemicals in the same group. Therefore, these compounds will be a basis for our next study. In every optimized structure, the nitro-furan group was shown to be stably bound to two Mg²⁺ ions as shown in Figure 2. The oxygen atom on the furan ring is also oriented toward the divalent metals, while the coordination force seems weak. Carbonyl oxygen at the ester linkage connecting to the furan ring is strongly coordinated to Mg²⁺ ion. Therefore, a large ring-shaped configuration of –O–C–N–O–Mg–Mg–O–C–C– is formed. In compound **3**, the inter-atomic distance of the two Mg²⁺ ions is 4.4 Å. The distance between the nitro-oxygen atom and one Mg²⁺ ion is 2.3 Å, and that between carbonyl oxygen and the other Mg²⁺ ion is 2.2 Å. The pentyl group positioned at the opposite side of the compound sticks out from the binding pocket. Hence, there is much room for improvement in this hydrophobic region. The oxygen atom at the amide bond has a noticeable interaction with the hydroxyl group of Ser499 of the RNase H domain. In compound **7**, the distance between the two Mg²⁺ ions is 3.8 Å. The distance between the nitro-oxygen and one Mg²⁺ ion is 2.0 Å, and that between carbonyl oxygen and the other Mg²⁺ ion is 2.1 Å. The polar atoms composing the amide bond have an interaction with the RNase H domain. In compound **10**, the distance between the two Mg²⁺ ions is 4.3 Å. The distance between nitro-oxygen and one Mg²⁺ ion is 2.1 Å, and that between carbonyl oxygen and the other Mg²⁺ ion is 2.3 Å. The oxygen atom at the amide bond has an interaction with Ser499 of the RNase H domain, while the large hydrophobic moiety at the side part is positioned outside the binding pocket. The QM/MM calculations confirmed that all of the compounds; **3**, **7** and **10**, can be stably bound to the active site of the RNase H domain

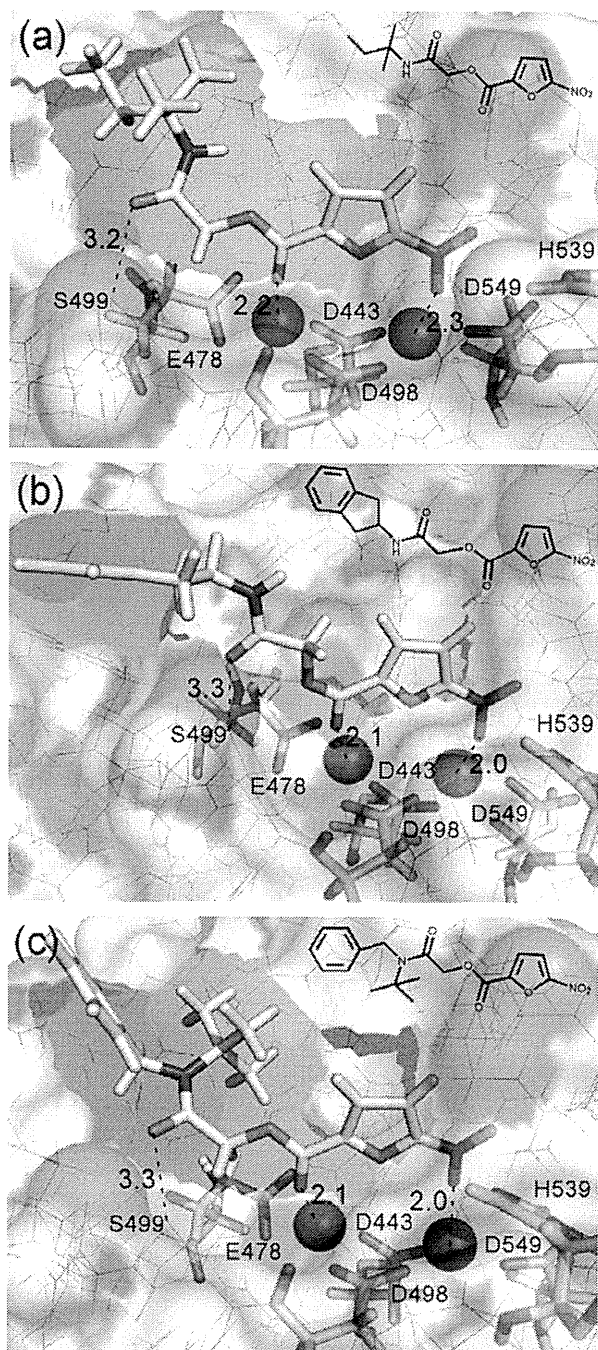


Figure 2. Optimized binding structures of the active compound to the RNase H domain, obtained by QM/MM calculation. (a), (b) and (c) correspond to compounds (3), (7) and (10), respectively. Chemical structures of the compounds are shown at the right top. Inhibitor compound and several polar residues are shown in stick representation. Two Mg^{2+} ions are denoted by spheres. Inter-atomic distances are shown in units of Å.

with coordinating to two divalent metal ions, while the interaction of other moiety is moderate.

Close observation of the optimized geometry by QM/MM calculation indicates that there is some space between the RNase H domain and inhibitory compounds around the ether oxygen at the ester linkage. This suggests that a few water molecules occupy the space when the compounds are bound to the RNase H domain.

There exists a polar residue, Ser499, deep inside at this space on the RNase H domain. This residue would have little influence on the function of RNase H. Therefore, one of the designs to improve inhibitory activity is to modify the compound to bear some polar functional group that can interact with Ser499. Substitution of ether oxygen with nitrogen or carbon atom to enable the incorporation of a polar functional group is one of the possible conversions of our derivatives to enhance binding affinity to the RNase H domain.

The difficulty in developing an RNase H inhibitor for practical use lies in the specificity and toxicity. In spite of much effort to enhance the inhibitory potency, the 50% inhibitory concentrations of many compounds reported so far are still in the order of sub-micromolar and they often lack sufficient specificity for HIV-1 RT-associated RNase H activity. Most problematically, they sometime display cytotoxicity to mammalian cells. Many previous compounds have shown little inhibitory activity in an in vitro cell culture replication assay. The derivatives synthesized in this work have a scaffold different from that of the previously reported inhibitors. It was shown in our previous study¹⁷ that the inhibitory potency of the hit chemical was highly specific to RNase H of retrovirus and the hit chemical further displayed an inhibitory activity in a cell culture replication assay. The present study showed that our derivatives had little cytotoxicity and that the chemical conversion at a part other than the 5-nitro-furan-2-carboxylic moiety increased the inhibitory activity. Moreover, there is still much room for modulation of the chemical structure. Accordingly, the analogues bearing the scaffold addressed in this study are good candidates for anti-HIV-1 drugs acting on RT-associated RNase H.

5. Summary

RNase H activity of reverse transcriptase is an attractive target of an antiviral agent for HIV-1 that is not yet addressed by currently approved drugs. A series of chemical compounds were synthesized on the basis of a hit chemical found in our previous in vitro screening. Inhibition of RNase H enzymatic activity was measured in a biochemical assay with a real-time fluorescence monitoring technique. Conversion of the nitro-furan group into other chemical structures drastically decreased the inhibitory activity except for nitro-thiophene. This means that the structural basis of nitro-furan is indispensable for inhibitory activity induced by analogues of the hit chemical. No notable change was observed in inhibitory potency when the hydrophobic moiety located at the opposite part of nitro-furan was modulated. This indicates that the modulated region has little interaction with the RNase H domain. Theoretical calculation with QM/MM method suggested the binding mode of the synthesized compounds to RNase H reaction active site. The characteristic property of the nitro-furan group is large electric polarity. Since oxygen atoms are negatively charged, these oxygen atoms will be strongly coordinated to divalent metal ions of the active site. The findings obtained in this work will be informative for designing potent inhibitors of RNase H enzymatic activity.

Acknowledgments

This work was supported by a Health and Labor Science Research Grant for Research on Publicly Essential Drugs and Medical Devices from the Ministry of Health and Labor of Japan. A part of this work was also supported by a Grant-in-Aid for Scientific Research (C) from Japan Society for the Promotion of Science (JSPS). Theoretical calculations were performed at the Research Center for Computational Science, Okazaki, Japan and at the Information Technology Center of the University of Tokyo and also by the high-performance computer system at Institute for Media Information Technology in Chiba University.

Supplementary data

Supplementary data associated with this article can be found, in the online version, at doi:10.1016/j.bmc.2010.12.011.

References and notes

- Sarafianos, S. G.; Das, K.; Hughes, S. H.; Arnold, E. *Curr. Opin. Struct. Biol.* **2004**, *14*, 716.
- Klumpp, K.; Mirzadegan, T. *Curr. Pharm. Des.* **2006**, *12*, 1909.
- Borkow, G.; Fletcher, R. S.; Barnard, J.; Arion, D.; Motakis, D.; Dmitrienko, G. I.; Parniak, M. A. *Biochemistry* **1997**, *36*, 3179.
- Tramontano, E.; Esposito, F.; Bads, R.; Di Santo, R.; Costi, R.; La Colla, P. *Antiviral Res.* **2005**, *65*, 117.
- Tarrago-Litvak, L.; Andreola, M. L.; Fournier, M.; Nevinsky, G. A.; Parissi, V.; de Soultrait, V. R.; Litvak, S. *Curr. Pharm. Des.* **2002**, *8*, 595.
- Kirschberg, T. A.; Balakrishnan, M.; Squires, N. H.; Barnes, T.; Brenda, K. M.; Chen, X.; Eisenberg, E. J.; Jin, W.; Kutty, N.; Leavitt, S.; Licican, A.; Liu, Q.; Liu, X.; Mak, J.; Perry, J. K.; Wang, M.; Watkins, W. J.; Lansdon, E. B. *J. Med. Chem.* **2009**, *52*, 5781.
- Himmel, D. M.; Maegley, K. A.; Pauly, T. A.; Bauman, J. D.; Das, K.; Dharia, C.; Clark, A. D., Jr.; Ryan, K.; Hickey, M. J.; Love, R. A.; Hughes, S. H.; Bergqvist, S.; Arnold, E. *Structure* **2009**, *17*, 1625.
- Su, H. P.; Yan, Y.; Prasad, G. S.; Smith, R. F.; Daniels, C. L.; Abeywickrema, P. D.; Reid, J. C.; Loughran, H. M.; Kornienko, M.; Sharma, S.; Grobler, J. A.; Xu, B.; Sardana, V.; Allison, T. J.; Williams, P. D.; Darke, P. L.; Hazuda, D. J.; Munshi, S. *J. Virol.* **2010**, *84*, 7625.
- Moelling, K.; Schulze, T.; Diringer, H. *J. Virol.* **1989**, *63*, 5489.
- Loya, S.; Hizi, A. *J. Biol. Chem.* **1993**, *268*, 9323.
- Tan, C. K.; Civil, R.; Mian, A. M.; So, A. G.; Downey, K. M. *Biochemistry* **1991**, *30*, 4831.
- Davis, W. R.; Tomsho, J.; Nikam, S.; Cook, E. M.; Somand, D.; Peliska, J. A. *Biochemistry* **2000**, *39*, 14279.
- Himmel, D. M.; Sarafianos, S. G.; Dharmasena, S.; Hossain, M. M.; McCoy-Simandle, K.; Ilina, T.; Clark, A. D., Jr.; Knight, J. L.; Julias, J. G.; Clark, P. K.; Krogh-Jespersen, K.; Levy, R. M.; Hughes, S. H.; Parniak, M. A.; Arnold, E. *ACS Chem. Biol.* **2006**, *1*, 702.
- Shaw-Reid, C. A.; Munshi, V.; Graham, P.; Wolfe, A.; Witmer, M.; Danzeisen, R.; Olsen, D. B.; Carrol, S. S.; Embrey, M.; Wai, J. S.; Miller, M. D.; Cole, J. L.; Hazuda, D. J. *J. Biol. Chem.* **2003**, *278*, 2777.
- Hang, J. Q.; Rajendran, S.; Yang, Y.; Li, T.; In, P. W. K.; Overton, H.; Parkes, K. E. B.; Cammack, N.; Martin, J. A.; Klumpp, K. *Biochem. Biophys. Res. Commun.* **2004**, *317*, 321.
- Budihis, S. R.; Gorshkova, I.; Gaidamakov, S.; Wamiru, A.; Bona, M. K.; Parniak, M. A.; Crouch, R. J.; McMahon, J. B.; Beutler, J. A.; Le Grice, S. F. *Nucleic Acids Res.* **2005**, *33*, 1249.
- Fuji, H.; Urano, E.; Futahashi, Y.; Hamatake, M.; Tatsumi, J.; Hoshino, T.; Morikawa, Y.; Yamamoto, N.; Komano, J. *J. Med. Chem.* **2009**, *52*, 1380.
- Davies II, J. F.; Hostomska, Z.; Hostomsky, Z.; Jordan, S. R.; Matthews, D. A. *Science* **1991**, *252*, 88.
- Klumpp, K.; hang, J. Q.; Rajendran, S.; Yang, Y.; Derosier, A.; Wong Kai In, P.; Overton, H.; Parkes, K. E.; Cammack, N.; Martin, J. A. *Nucleic Acids Res.* **2003**, *31*, 6852.
- Bauman, J. D.; Das, K.; Ho, W. C.; Baweja, M.; Himmel, D. M.; Clark, A. D., Jr.; Oren, D. A.; Boyer, P. L.; Hughes, S. H.; Shatkin, A. J.; Arnold, E. *Nucleic Acids Res.* **2008**, *36*, 5083.
- Parniak, M. A.; Min, K. L.; Budihis, S. R.; Le Grice, S. F.; Beutler, J. A. *Anal. Biochem.* **2003**, *322*, 33.
- Chan, K. C.; Budihis, S. R.; Le Grice, S. F.; Parniak, M. A.; Crouch, R. J.; Gaidamakov, S. A.; Isaaq, H. J.; Wamiru, A.; McMahon, J. B.; Beutler, J. A. *Anal. Biochem.* **2004**, *331*, 296.
- Li, H.; Robertson, A. D.; Jensen, J. H. *Proteins* **2005**, *61*, 704.
- Vreven, T.; Morokuma, K.; Farkas, Ö.; Schlegel, H. B.; Frisch, M. J. *J. Comp. Chem.* **2003**, *24*, 760.
- Frisch, M. J.; Trucks, G. W.; Schlegel, H. B.; Scuseria, G. E.; Robb, M. A.; Cheeseman, J. R.; Montgomery, J. A., Jr.; Vreven, T.; Kudin, K. N.; Burant, J. C.; Millam, J. M.; Iyengar, S. S.; Tomasi, J.; Barone, V.; Mennucci, B.; Cossi, M.; Scalmani, G.; Rega, N.; Petersson, G. A.; Nakatsuji, H.; Hada, M.; Ehara, M.; Toyota, K.; Fukuda, R.; Hasegawa, J.; Ishida, M.; Nakajima, T.; Honda, Y.; Kitao, O.; Nakai, H.; Klene, M.; Li, X.; Knox, J. E.; Hratchian, H. P.; Cross, J. B.; Bakken, V.; Adamo, C.; Jaramillo, J.; Gomperts, R.; Stratmann, R. E.; Yazyev, O.; Austin, A. J.; Cammi, R.; Pomelli, C.; Ochterski, J. W.; Ayala, P. Y.; Morokuma, K.; Voth, G. A.; Salvador, P.; Dannenberg, J. J.; Zakrzewski, V. G.; Dapprich, S.; Daniels, A. D.; Strain, M. C.; Farkas, O.; Malick, D. K.; Rabuck, A. D.; Raghavachari, K.; Foresman, J. B.; Ortiz, J. V.; Cui, Q.; Baboul, A. G.; Clifford, S.; Cioslowski, J.; Stefanov, B. B.; Liu, G.; Liashenko, A.; Piskorz, P.; Komaromi, I.; Martin, R. L.; Fox, D. J.; Keith, T.; AlLaham, M. A.; Peng, C. Y.; Nanayakkara, A.; Challacombe, M.; Gill, P. M. W.; Johnson, B.; Chen, W.; Wong, M. W.; Gonzalez, C.; Pople, J. A. *GAUSSIAN 03*; Gaussian, Inc.: Wallingford, CT, 2004.
- Smith, J. S.; Roth, M. J. *J. Virol.* **1993**, *67*, 4037.
- Sarafianos, S. G.; Das, K.; Tantillo, C.; Clark, A. D., Jr.; Ding, J.; Whitcomb, J. M.; Boyer, P. L.; Hughes, S. H.; Arnold, E. *EMBO J.* **2001**, *20*, 1449.
- Huang, H.; Chopra, R.; Verdine, G. L.; Harrison, S. C. *Science* **1998**, *282*, 1669.
- Katayanagi, K.; Okumura, M.; Morikawa, K. *Proteins* **1993**, *17*, 337.
- De Vivo, M.; Dal Peraro, M.; Klein, M. L. *J. Am. Chem. Soc.* **2008**, *130*, 10955.

Mechanism of Drug Resistance of Hemagglutinin of Influenza Virus and Potent Scaffolds Inhibiting Its Function

Hiroshi Yanagita,^{†,‡} Norio Yamamoto,^{‡,§,‡,*} Hideyoshi Fuji,[†] Xinli Liu,[†] Masakazu Ogata,[†] Mizuho Yokota,[†] Hiroshi Takaku,^{||} Hideki Hasegawa,[⊥] Takato Odagiri,[‡] Masato Tashiro,[‡] and Tyuji Hoshino^{†,*}

[†]Graduate School of Pharmaceutical Sciences, Chiba University, Inohana 1-8-1, Chuo-ku, Chiba 260-8675, Japan

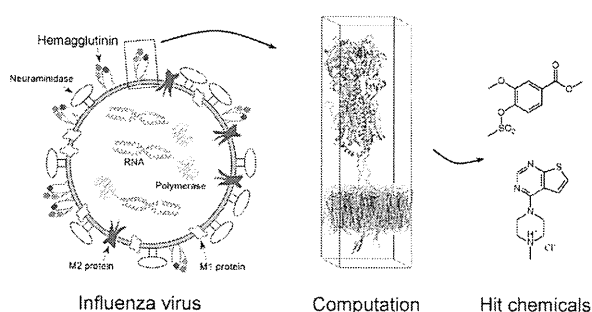
[‡]Influenza Virus Research Center and [⊥]Department of Pathology, National Institute of Infectious Diseases, 4-7-1 Gakuen, Musashimurayama, Tokyo 208-0011, Japan

[§]Department of General Medicine, Juntendo University School of Medicine, 2-1-1 Hongo, Bunkyo-ku, Tokyo 113-8421, Japan

^{||}Department of Life and Environmental Science, Chiba Institute of Technology, 2-17-1 Tsudanuma, Narashino-shi, Chiba 275-0016, Japan

Supporting Information

ABSTRACT: Highly pathogenic influenza viruses have become a global threat to humans. It is important to select an effective therapeutic option suitable for the subtypes in an epidemic or pandemic. To increase the options, the development of novel antiviral agents acting on targets different from those of the currently approved drugs is required. In this study, we performed molecular dynamics simulations on a spike protein on the viral envelope, hemagglutinin, for the wild-type and three kinds of mutants using a model system consisting of a trimeric hemagglutinin complex, viral lipid membrane, solvation waters, and ions. A natural product, stachyflin, which shows a high level of antiviral activity specific to some subtypes of influenza viruses, was examined on binding to the wild-type hemagglutinin by docking simulation. The compound potency of stachyflin is, however, easily lost due to resistant mutations. From a comparison of simulation results between the wild-type and the resistant mutants, the reason for the drug resistance of hemagglutinin was clarified. Next, 8 compounds were selected from a chemical database by *in silico* screening, considering the findings from the simulations. Inhibitory activities to suppress the proliferation of influenza virus were measured by cell-based antiviral assays, and two chemical scaffolds were found to be potent for an inhibitor. More than 30 derivatives bearing either of these two chemical scaffolds were synthesized, and cell culture assays were carried out to evaluate the compound potency. Several derivatives displayed a high compound potency, and 50% effective concentrations of two synthesized compounds were below 1 μM .



Influenza viruses cause acute respiratory infection in humans that occasionally progresses to a severe pulmonary condition. Even seasonal epidemics account for 300,000 or more deaths per a year all over the world. Recently, the emergence of highly pathogenic avian and swine influenza viruses has become a global threat to humans. Avian influenza H5N1 virus infections have been reported since 2003,¹ and a pandemic of transmissible H5N1 virus is a serious concern for public health.² The recent outbreak of swine influenza subtype H1N1 resulted in considerable mortalities for infants and the elderly. While several anti-influenza drugs are currently approved, their effectiveness for pandemic viruses may be limited due to drug resistance. Therefore, the development of additional antiviral agents against influenza virus infection is needed.

The currently available anti-influenza drugs target one of two viral proteins: M2 protein and neuraminidase. M2 protein is embedded in the lipid membrane of the viral envelope and functions as an ion channel to pump protons into the viral particles. Amantadine and Rimantadine block the function of M2 protein by combining at the center of the channel or the side domain of this enzyme.^{3,4} Neuraminidase is a kind of spike protein sticking out on the viral particle surface. Neuraminidase causes the hydrolysis of neuraminic acid of the glycan of the host cell. Zanamivir, Oseltamivir, Peramivir, and Laninamivir have been used as neuraminidase inhibitors.^{5,6} Emergence of drug-resistant viruses has been reported for the above approved

Received: September 1, 2011

Accepted: January 4, 2012

Published: January 4, 2012

drugs. For example, resistance against Amantadine and Rimantadine was shown in the H3N2 and H1N1 viruses, and resistance against Oseltamivir was shown for the H1N1 virus.^{7–9} Since an RNA virus easily acquires amino acid mutations, the emergence rate of drug-resistant viruses is high. A drug-resistant virus is a serious issue in infectious diseases because a chemotherapeutic approach is restricted. In order to combat drug-resistant viruses, it is important to prepare many chemotherapeutic options and select an effective option suitable for subtypes in an epidemic. Accordingly, development of novel antiviral drugs that act on a target different from those of the currently approved drugs is needed.

A species of moss, *Stachybotrys s. RF-7260*, generates a unique natural product named stachyflin. Stachyflin was found to have strong antiviral activity against some subtypes of influenza viruses.^{10–12} The inhibitory mechanism of stachyflin is different from the inhibitory mechanism of the currently approved anti-influenza drugs. Stachyflin binds with hemagglutinin (HA) on the viral envelope and blocks conformational change of HA to prevent the lipid membrane of the viral envelope from merging with that of host cell. HA is one of the attractive targets of antiviral agents for the following reasons. First, HA is a key component in the viral fusion process that has no cellular counterparts and therefore has a potential advantage in selectivity and toxicity. Second, HA inhibitors will complement other currently approved drugs since they act on a different molecular target in the virus life cycle.

Stachyflin is highly effective for influenza virus of A/WSN/33 H1N1 subtype, and the 50% inhibitory concentration (IC_{50}) value for the WSN strain was reported to be 3 nM.¹² However, its inhibitory activity for other strains including other H1N1 virus strains is not so high, and its inhibitory activity is easily decreased by amino acid mutations of the virus. Since several amino acid mutations involved in drug resistance are not localized in one domain of HA, it is difficult to understand the mechanism of drug resistance caused by mutations straightforwardly. The chemical structure of stachyflin is complicated. Five rings merge to form a structure called the 3*H*-naphthopyrano-isoindol-3-one scaffold, and stachyflin also contains five chiral centers (Figure 1a). This complexity in its chemical structure is another reason for the difficulty in improving compound potency for stachyflin derivatives.

Yoshimoto and co-workers performed an experiment on resistance induction with stachyflin¹³ and demonstrated that K51R, K121E, S206L in the HA2 subunit and V176I in the HA1 subunit appeared in resistant viruses (Figure 1b). K51R and K121E mutations were suggested to be essential for drug resistance. They suggested from a docking simulation that stachyflin was bound to a position close to Lys51 or Phe110 of HA. This simulation, however, provided no clear explanation for the mechanism of drug resistance due to the above amino acid mutations. The mechanism of the drug resistance of HA should be clarified for producing promising inhibitory compounds.

In this study, we performed computational analysis, screening to find candidate compounds, a cell-based antiviral assay, and synthesis of analogue compounds in the following manner: (1) Molecular dynamics (MD) simulations were carried out for the wild-type and three kinds of variants containing amino acid mutations responsible for drug resistance in order to clarify the mechanism. (2) A point for designing a potential inhibitor was deduced from the concept of minimizing the influence of the drug-resistance-related conformational change of HA. (3) An *in*

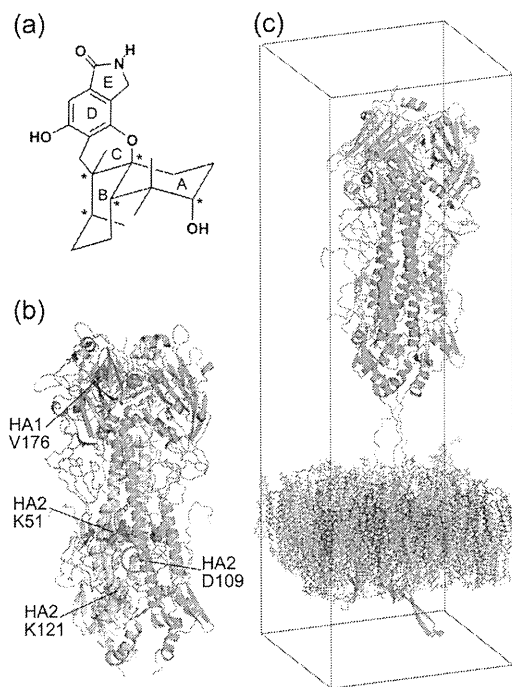


Figure 1. (a) Chemical structure of stachyflin. Stachyflin is composed of five complex rings and contains five chiral centers. The rings are labeled A–E, and chiral carbon atoms are marked by asterisks. (b) Structure of hemagglutinin in a trimer conformation. Spheres denote the residues introducing amino mutations in the respective mutants. The center residue targeted in the ligand docking simulation is indicated by a circle. (c) Calculation model of a complex of hemagglutinin trimer and lipid membrane. Hemagglutinin subunits HA1 and HA2 are colored blue and green, respectively. The membrane consists of 6 different kinds of lipid molecules, and its composition is presented in Supplementary Table S1. No water molecules or ions are shown for visual clarity.

silico screening was performed to find low-molecular-weight compounds showing inhibitory activity against HA, considering the above point and using the pharmacophore of stachyflin. (4) A cell-based assay was carried out to evaluate the inhibitory potencies of the compounds collected by the *in silico* screening. (5) Derivatives of the hit compounds found from the screening were synthesized, and their inhibitory activities were measured to elucidate the antiviral potency of the scaffold proposed in this work.

RESULTS AND DISCUSSION

Structural Difference in HA between the Wild-Type and Mutants. MD simulation was carried out for 30 ns to obtain the probable protein structure of HA in a trimer form for the wild-type and three mutants, using the model system containing a trimeric hemagglutinin and viral lipid membrane as shown in Figure 1c. The respective mutants contain the resistant mutations K51R and K121E in HA2 for mutant 1, V176I in HA1 and K51R, K121E in HA2 for mutant 2, and V176I in HA1 and K51R in HA2 for mutant 3. Root mean square deviation (rmsd) relative to the structure after heating is shown in Supplementary Figure S1. The rmsd value for the wild-type (Figure S1a) was scarcely changed during 30 ns. Each of the rmsd curves for the mutants (Figures S1b–d) shows a

gradual increase up to 15 ns and seems to be almost constant after 20 ns. Plots of rmsd in Figure S1 were obtained from the coordinates of main chain atoms of the whole HA. The N-terminal domain of the HA1 subunit is so flexible that rmsd values are considerably large. Hence, rmsd values were calculated again with respect to the main chain atoms of only the HA2 subunit with excluding the C-terminal region, aa 176–222. The rmsd curves only for HA2 in Supplementary Figure S2 also became constant after 20 ns for every model. Accordingly, protein conformations for the respective models were judged to be equilibrated.

Principal component analysis (PCA) in Supplementary Figure S3 indicates that the trajectory structures for the last 5 ns are in a single conformation for every model. The equilibration of the simulation is also confirmed from these PCA plots. In order to extract the plausible protein structure, the averaged structure was obtained using 500 trajectory structures from the last 5 ns of MD simulation. The rmsd between each trajectory structure and the average structure was calculated, and then one trajectory structure with the smallest rmsd value was determined to be the plausible protein structure. At a glance, there is no prominent difference among the 4 models in terms of shape of the trimer, conformation of the HA1 and HA2 subunits, or position of helices. Although no significant apparent change is seen in the backbone of HA, there appears a notable difference in the location of side chains. The differences in the side chain will be responsible for the change in binding affinity and inhibitory activity of inhibitors.

Binding of an Inhibitor to HA. By means of docking simulation, an inhibitor, stachyflin, was bound to the HAs, using the respective plausible protein structures obtained by MD calculations. In the wild-type HA, stachyflin was bound near Asp109 of the HA2 subunit (Figure 2). Hydrophobic interactions were observed between the B ring of stachyflin and Phe37 of HA1, between the C ring of stachyflin and Phe110 of HA2, and between the D ring and Leu113. Hydrogen bonds were formed between the O atom on the D ring of stachyflin and the amino group of Asn114 in HA2 and between the O atom on the E ring and the amino group of Asn117.

In mutant 2, stachyflin was bound to a location similar to that of the wild-type (Supplementary Figure S4c), while the docking simulation showed binding of stachyflin at the central space among three helices of the HA2 trimer in mutants 1 and 3 (Figures S4b and d). Judging from the binding affinity evaluated by ASP score function (Supplementary Table S2), the binding of stachyflin to the wild-type HA is the most stable. All of the mutants showed notable decrease in binding affinity compared to that of the wild-type.

An amino acid mutation of K51R in HA2 commonly appeared in the three mutants, suggesting that K51R was the primary mutation for drug resistance. Other mutations, K121E and V176L, will enhance the resistance. All of these amino mutations are, however, distant from the stachyflin binding site. Our MD simulation clearly indicated that inner helices of HA2 subunit were rotated (Figure 3a). One of the three inner helices, chain D in nomenclature in PDB 1RD8, was rotated by 10.8° in mutant 1 and by 15.0° in mutant 2 compared to the wild-type (Figure 3b). The amino group on the side chain of Lys51 makes a strong hydrogen bond with the hydroxy group of Thr107 of HA2 (Figure 3c). Arg is also a positively charged amino acid residue, but the length of the side chain is longer than that of Lys. When Lys is converted into Arg, the side chain

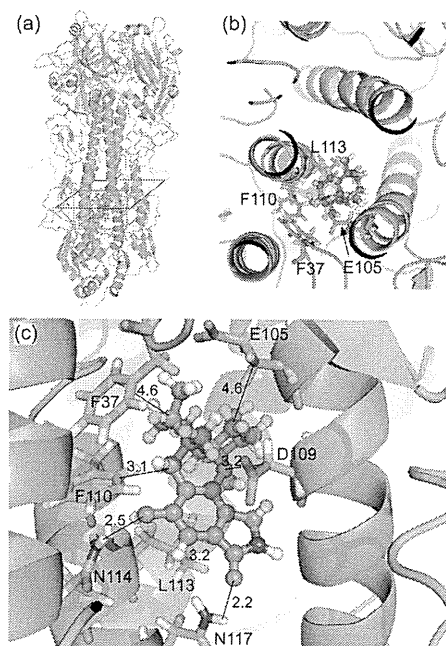


Figure 2. (a) Complex structure of stachyflin and hemagglutinin obtained by the ligand docking simulation. (b) Binding site of stachyflin viewed in a plane perpendicular to the helices of the HA2 subunit. (c) Binding mode of stachyflin, shown in a magnified view of the area indicated by a red frame in panel a. Stachyflin is bound to the space between two helices of HA2 subunit, making strong interaction with side chains of Asp109, Phe110, and Leu113. The interaction distances are in Å.

of the residue at codon 51 expands and pushes T107. The side chain of Thr107 serves as a lever to rotate the helix. The position of the side chain of Asp109 is largely deviated from that of the wild-type because of the closeness to Thr107. Lys121 has a strong interaction with the carboxy group of Asp18 of the HA1 subunit. When Lys is converted into Glu in the K121E mutation, the side chain of Glu121 and Asp18 of HA1 causes repulsion to increase the distance between them. This repulsion assists the helix rotation, and the deviation of Leu113 and Asn114 from the wild-type will be enhanced because of the closeness to Glu121. To monitor the helix rotation, the angle between the line connecting the C α and C β atoms of Asp109 on the inner helix chain D and the line connecting the Asp109 C α atom on chain D and the Phe110 C α atom on another inner helix chain B was measured through the simulation as shown in Supplementary Figure S5. A significant angle change was observed after 10 ns for every model. The distances between the N ζ atom of Lys51 (or C ζ in K51R) of HA2 and the O γ atom of Thr107 of HA2 and also between the N ζ atom of Lys121 (or C δ in K121E) of HA2 and C γ of Asp18 of HA1 were monitored as shown in Supplementary Figure S6. Because HA is a trimer and there exist three HA1 and three HA2 subunits in the calculation models, three combinations of those interatomic distances were measured through the simulation. The distance plots in Figure S6 indicate that the interaction between the residues at codon 51 and codon 107 is quite stable in the wild-type HA. In contrast, some of these distances occasionally increased in the mutants. The distance between the residues at codon 121 of HA2 and at codon 18 of HA1 ceaselessly fluctuated in all

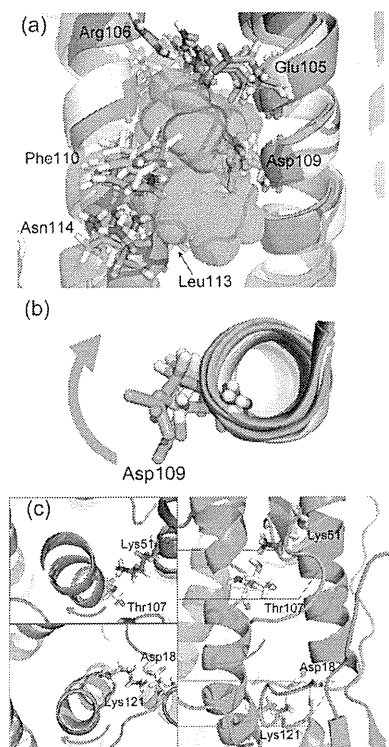


Figure 3. (a) Superposition of the hemagglutinin structures of mutants on that of the wild-type. The wild type is colored green and mutants 1, 2, and 3 are colored cyan, magenta, yellow, respectively. The binding area of stachyflin to the wild-type HA is shown in a mesh representation. There is no significant change in positions of helices. However, the amino acid mutations cause rotation of helices. The rotation angle is estimated from the position of C β atom of Asp109, as shown in panel b. Thr107 in HA2 subunit and Asp18 in HA1 subunit are deeply involved in the helix rotation induced by K51R and K121E mutations, respectively, as shown in panel c. Two illustrations on the left side are depicted around the planes perpendicular to the helices and containing Thr107 or Lys121, respectively. The planes are indicated by blue and red frames in the right side illustration in panel c.

models. A strong interaction was, however, established at least for one combination of Lys121 and Asp18 in the wild-type.

The helix rotation pointed out above is the reason for the decrease in inhibitory activity of stachyflin to the resistant mutants. In the mutants, the side chains of Asp109 and Leu113 are displaced and occupy the space that stachyflin was bound to in the wild-type HA. The side chains of Phe110 and Asn114 are also displaced and move away from the stachyflin binding site as shown in Supplementary Figure S7. Therefore, stachyflin would not be bound to HA stably any more. The helix rotation in mutant 3 is small. This is naturally understood because the influence of V176I mutation in the HA1 subunit is slight. This finding suggests that some degree of flexibility is favorable to HA inhibitors for releasing the strain due to the helix rotation. Therefore, compounds bearing a complicated heteroring structure are disadvantageous. Instead, a single bond connection of separated ring domains can be a good chemical frame to maintain structural flexibility.

Conformational change accompanying helix rotation has been reported for other kinds of transmembrane proteins. For example, an X-ray crystallographic analysis of the human β 2

adrenergic G-protein-coupled receptor¹⁴ suggested that a rotational motion was observed for one of the transmembrane helices owing to the binding of a ligand for the receptor. An electron paramagnetic resonance measurement¹⁵ and a computational analysis¹⁶ indicated that light adsorption induced a conformational change of retinal chromophore in sensory rhodopsin and this conformational change caused the rotation of transmembrane helix TM1 to lead signal transduction of the sensory protein.

Search for Active Compounds. The natural product stachyflin possesses a unique pentacyclo structure in which each ring is labeled as A, B, C, D, and E, respectively. Rings AB are composed of a naphthol skeleton, and rings DE are composed of an indol frame. Ring C bears a pyran structure and connects rings AB and rings DE. Rings ABC are fused in *cis*-form, and the oxygen of pyran is bonded to the carbon at the junction of rings AB. Furthermore, stachyflin contains 5 chiral centers, in which all of the chiral carbons are located on rings AB. Therefore, the naphthol moiety and its connection to pyran make the chemical structure of stachyflin highly complicated. A hydroxy group and carbonyl oxygen are bound to the indol ring, which characterizes the electrostatic property of stachyflin. The hydroxy group of naphthol is another factor to characterize the polar feature of this natural product.

Eight chemical compounds were selected by an *in silico* screening using the pharmacophore of stachyflin (Table 1). All of the selected compounds were produced by organic synthesis and are available by purchase. The molecular weights of these compounds range from 304 to 341. Compound 1 bears two ester bonds and a benzofuran moiety corresponding to rings C and D of stachyflin in superimposition. Compound 2 bears a thieno-pyrimidine, which corresponds to rings D and E of stachyflin and a phenyl-cyclopentane corresponding to rings A and B. Two benzene rings are connected *via* a dichloromethyl-carbonyl group in compound 3. Methylbenzoic acid methyl-ester in compound 4 corresponds to rings D and E, and dimethyl-diazolane is connected by a sulfonyloxy group. Thieno-pyrimidine in compound 5 corresponds to rings D and E, and another thiophene corresponds to ring A. The molecular weight of compound 6 is the largest among the selected compounds, and methylester-benzene corresponds to rings D and E and pyridyl-triazole corresponds to rings A and B. Compound 7 bears a seven-membered ring containing two nitrogen atoms. Hydroxybenzene in compound 8 corresponds to ring B of stachyflin.

Assay for Antiviral Activity. The 8 selected compounds were tested in an influenza virus cell culture assay (Table 1). Compounds 4 and 5 were found to have significant antiviral activity ($EC_{50} < 5 \mu M$). Although compound 2 was the most highly potent with an EC_{50} of $3 \mu M$, compound 2 exhibited significant cytotoxicity at a concentration of $6 \mu M$, measured by an MTT assay with MDCK cells. Since compounds 4 and 5 showed no noticeable cytotoxicity, these two compounds were chosen as the structural core in the next step for organic synthesis.

The binding modes of compounds 4 and 5 to the wild-type HA were predicted by performing docking simulation. The most probable docking structures are shown in Figure 4a and b, which were determined from the score ranking for 50 docking poses. The two compounds are bound to almost the same position as stachyflin is. That is, these compounds are located not in the central space of HA2 trimer but at a position in the middle of two helices of the HA2 subunit. The calculated

Table 1. Structures and Inhibitory Activities of the Chemical Compounds Obtained through an *in Silico* Screening

Compound	Structure	Superimposition ^{a)}	EC ₅₀ (μM)	CC ₅₀ (μM)
1			9.0	> 60
2			3.0 >	5.9
3			> 32	> 60
4			4.4	> 60
5			4.9	> 60
6			17.9	> 60
7			31.4	> 60
8			14.9	> 60

^aStachyflin is depicted in green stick representation, while compounds are blue.

binding affinities of these two compounds in ASP score are lower than that of stachyflin (TSupplementary table S2) but higher than that in the cases of stachyflin bound to the three kinds of mutants.

Synthesis of Analogue Compounds. Compound 4 bears a structural core of vanillic acid. Based on the vanillic acid methylester core, 22 derivatives from compound 4 were synthesized as shown in Table 2, where the functional group at the fourth position of the benzoic acid was modulated. A highly potent compound (9) was found in the analogues in which methylsulfonyl was connected to the fourth position. The incorporation of benzyl or methylphenyl (10, 12) showed no inhibitory activity, while moderate activity was observed in case of phenyl only (11). This means that a small chemical group is favorable for the substitute connecting *via* the sulfonyloxy group. Conversion of the sulfonyl group into an ester bond (13–15) resulted in complete loss of compound potency, regardless of the size of the substitutes connected to

the ester. Substitution of the sulfonyl group by an alkyl chain (16–20) resulted in loss of inhibitory activity. Only compound 18 in which the sulfonyl group was substituted by benzyl showed slight inhibitory activity. Then the effect of addition of functional groups to the benzyl (21–28) was surveyed. Compound 22 containing an oxybenzyl group at the *para*-position of the benzyl exhibited high compound potency. The inhibitory activity was maintained with the addition of methoxy or trifluoromethyl at the *para*-position, while the incorporation of other kinds of functional groups (23–25) or the addition of trifluoromethyl at the *ortho*- or *meta*-position (27, 28) resulted in loss of inhibitory activity. Conversion of the sulfonyloxy group into an amino group (29, 30) was tested. None of the derivatives showed noticeable increase in compound potency.

Compound 5 bears a heteroring core of thieno-pyrimidine, and a dimethyl-aminy-thienyl group is connected to the heteroring *via* amine. Keeping the heteroring core, 9 derivatives from compound 5 were synthesized as shown in Table 3. The

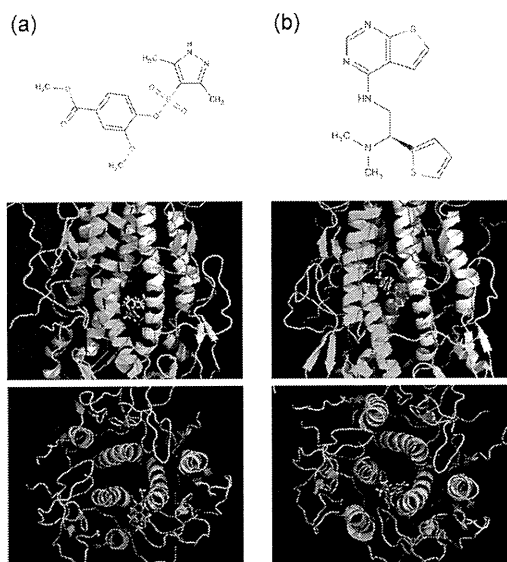


Figure 4. Hit chemicals found through *in silico* screening: (a) compound 4 and (b) compound 5. Top: chemical structure. Middle: binding site of the compound predicted by the docking simulation. Bottom: binding position of the compound viewed from the direction of subunit HA1.

introduction of benzyl *via* amine group (31) resulted in an increase in inhibitory activity. In contrast, conversion into dimethylamine (32, 33) resulted in loss of compound potency. Interestingly, while conversion into methyl-piperazine (34) resulted in a decrease in inhibitory activity, its hydrochloride salt (35) exhibited a high compound potency. Phenyl-piperazine (36) also exhibited a considerably high inhibitory activity. The conversion of thiophene of compound 5 into benzene (37) exhibited a high compound potency, while its chiral analogue (38) showed no inhibitory activity. This chiral-selective compound potency was confirmed by substitution of a Boc protection group (39) for the dimethylamine of compound 37.

Actions of Active Compounds for Blocking HA. Fusion of the membrane is an essential process in the entry of influenza virus into the host cell. HA mediates this process through two functions in the early stage of the viral life cycle.¹⁷ One is anchoring at sialylated glycoprotein receptors on the cell membrane surface. The other is the low-pH induced conformational change that initiates the exposure of a fusion peptide, a hydrophobic N-terminal segment buried in the HA trimer interface, to be inserted into the endosomal membrane. Stachyflin is assumed to block this fusogenic process of HA.^{12,13} Indeed, in the predicted binding structure shown in Figure 2, stachyflin is combined with HA with the formation of two strong hydrogen bonds and three strong aromatic ring-involved hydrophobic interactions.

Several other compounds blocking the fusogenic activity of HA have been identified.^{18–22} An active compound¹⁸ bears a naphthoquinone skeleton, which is commonly seen in stachyflin as rings AB. Another compound¹⁹ contains a quinolizin moiety connected to a benzamide skeleton, and a one-step virus growth experiment indicated that this compound mainly inhibited virus proliferation at the early stage of the replication cycle. Therefore, a quinoline skeleton is one of the effective chemical cores for binding to HA. A compound

containing piperadine connected to trifluoro-methylbenzoyl also showed high inhibitory activity for influenza virus replication.²⁰ Ligand docking calculation suggested that this compound was bound to a site near Phe110 of the HA2 subunit, which is almost identical to the binding site of stachyflin obtained in this work as shown in Figure 2. A compound analogue to podocarpic acid was identified as an inhibitor of type A viruses²¹ and showed a high inhibitory activity especially for Kawasaki strain but was not so sensitive to WSN strain. In contrast, some recently identified blockers are targeted at another domain of HA.^{23,24} Some peptides mimicking sialic acid were shown to inhibit the entry of viruses into host cells, attached to the receptor-binding site of HA.²³ Synthesized macromolecules containing three sialyllactoses linked with trisphenol or trisaniline were reported to inhibit viral replication, combined with the receptor-binding site of HA.²⁴ Recently, an HA inhibitor bearing a benzenesulfonamide core was identified through structural modifications of a salicylamide derivative.²⁵ It is interesting to note that the chemical structure of this agent resembles that of compound 9 in Table 2 to some extent.

In most of the active compounds, susceptibility varies among strains of influenza viruses and the inhibitory activity is drastically decreased due to the acquirement of resistant mutation. Our MD simulation demonstrated that the rotation of helices is the reason for the reduction of compound potency. Due to the increase in performance of computers and the development of calculation methodology, several computational analyses have recently been carried out.^{26–32} Quantum mechanical calculations using the fragment molecular orbital method were used to investigate the role of key amino acid residues in recognizing sialoglycoproteins on the host cell surface²⁶ or in combining with neutralizing monoclonal antibodies.²⁷ Huge MD simulations were performed to examine the interaction between HA and sialoglycans²⁸ and clarify the reason for mutations at the receptor-recognizing site.²⁹ MD simulations were also employed to evaluate the binding free energy³⁰ and to interpret the difference in receptor specificity.³¹ A computational approach was further demonstrated to be quite helpful for designing protein peptides that strongly inhibit the function of HA.³²

Pharmaceutical Properties of Hit Chemicals. Since stachyflin exhibits a highly potent anti-influenza activity for the wild-type WSN strain and is a challenging synthetic target due to its unique alkaloid structure, two research groups have so far attempted total synthesis of stachyflin. The first total synthesis of racemic (\pm)-stachyflin was reported by Taishi *et al.*,¹¹ in which the characteristic structure of 5 heterorings was built one by one in 29 steps. The first enantioselective total synthesis of (+)-stachyflin was recently achieved by Watanabe *et al.*,³³ utilizing an acid-induced domino epoxide-opening, rearrangement, cyclization reaction.³⁴ These synthetic studies suggest the possibility for producing stachyflin analogues and encourage the development of stachyflin-based antiviral agents. The complexity in synthesis is, however, disadvantageous from the viewpoint of productivity in manufacturing. Carey and co-workers analyzed the reactions used for the preparation of drug candidate molecules,³⁵ surveying 128 compounds produced in the departments of process chemistry of three major pharmaceutical companies. According to their analysis, the average number of chemical steps for synthesizing one candidate is 8.1. Compounds containing a chiral center account for about half of the 128 molecules. Therefore, the structural

Table 2. Structures and Inhibitory Activities of the Synthesized Analogues to Compound 4, Which Bears a Vanillic Acid Core^a

Compound	X	R	Temp. (°C)	Time (h)	Yield (%)	EC ₅₀ (μM)
9		OSO ₂ Me	rt	3	71	0.9
10	OH	OSO ₂ CH ₂ Ph	rt	3	75	>10
11		OSO ₂ Ph	rt	6	81	7.0
12		OSO ₂ <i>p</i> -MeC ₆ H ₄	rt	6	82	>10
13		OCOMe	rt	3	35	>10
14	OH	OCOCH ₂ Cl	rt	3	66	>10
15		OCOPh	reflux	3	80	>10
16			reflux	24	93	>10
17	OH	OCH ₂ <i>t</i> -Bu	reflux	72	21	>10
18		OCH ₂ Ph	rt	8	81	8.3
19		OCH ₂ CH ₂ Ph	reflux	24	70	>10
20		OCH ₂ (CH ₂) ₂ Ph	reflux	24	91	>10
21	OH	OCH ₂ <i>p</i> -MeOC ₆ H ₄	rt	12	72	8.1
22		OCH ₂ <i>p</i> -BnOC ₆ H ₄	rt	12	83	2.5
23		OCH ₂ <i>p</i> -NO ₂ C ₆ H ₄	rt	12	67	>10
24		OCH ₂ <i>p</i> -FC ₆ H ₄	rt	12	88	>10
25		OCH ₂ 2,3,4,5,6-F ₅ C ₆	rt	12	82	>10
26		OCH ₂ <i>p</i> -CF ₃ C ₆ H ₄	rt	12	79	8.2
27		OCH ₂ <i>o</i> -CF ₃ C ₆ H ₄	rt	12	76	>10
28		OCH ₂ <i>m</i> -CF ₃ C ₆ H ₄	rt	12	68	>10
29	NH ₂	NHCH ₂ Ph			54	8.5
30		N(CH ₂ Ph) ₂	rt	12	27	>10

^aCondition: (a) K₂CO₃, R-Cl, CH₃CN, temp, time, 21–93%.

core of stachyflin would not be suitable for scale-up synthesis in terms of the number of synthetic steps and the number of chiral centers. In this study, we provided two scaffolds exhibiting antiviral activity. Most of the compounds shown in Tables 2 and 3 were synthesized within 3 steps, except for compounds 37–39. Compounds 37–39 include chiral centers, and the synthesis of these compounds was achieved at most within 8 steps. Accordingly, the proposed scaffolds are feasible for diverse modulation of functional groups and then ones of the chemical bases for the development of HA inhibitors.

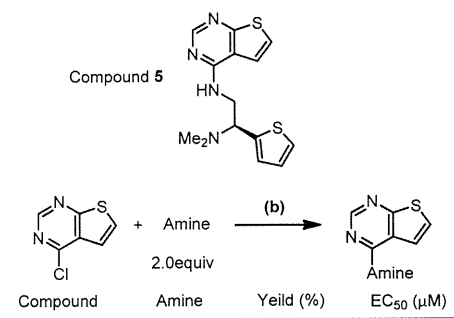
A requirement of antiviral drugs in clinical use is inhibitory activity for a broad range of viral strains. We tested the potency of several compounds synthesized in this study using A/Vietnam/1194/2004 (H5N1) strain,³⁶ which causes severe pathological conditions for humans and is one of the viruses attracting keen concern for the threat of a pandemic. A cell-based antiviral assay indicated that compounds 31 and 39 were effective for this H5N1 type virus with IC₅₀ values of 0.2 and 5.2 μM, respectively. This suggests that the scaffolds found in this study will maintain compound potency over different types of influenza viruses.

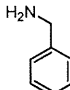
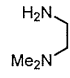
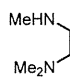
Plan of the Design of Potent Agents. In the *in silico* screening carried out in this study, 4 features, *i.e.*, hydrophobic region, hydrogen-bond donor, hydrogen-bond acceptor, and aromatic ring, were monitored for pharmacophore. Hit chemical compound 4 is compatible with stachyflin in the

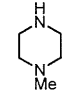
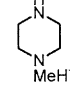
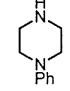
three features of aromatic ring, hydrophobic region, and hydrogen-bond acceptor. Hit chemical compound 5 is compatible in all four features. All of the 8 selected compounds are compatible with stachyflin at least in two features, aromatic ring and hydrogen-bond acceptor. That is, these two features are commonly observed in pharmacophores of all selected compounds. This suggests that aromatic ring and hydrogen-bond acceptor are indispensable for inhibitors analogous to stachyflin. From the viewpoint of compatibility in the pharmacophore, compound 5 is the most advantageous for an HA inhibitor. In the binding modes of compounds 4 and 5 to the wild-type HA shown in Figure 3, compound 4 generated three hydrogen bonds with HA. In contrast, one hydrogen bond was observed between compound 5 and HA. The binding position of compound 5 is considerably close to that of stachyflin. These findings in binding mode suggest that the shape complementarity between compound 5 and the binding site in HA is high, while electrostatic complementarity is more significant in the binding of compound 4.

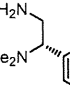
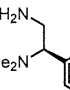
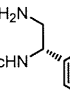
Methylester of compound 4 corresponds to carbonyl oxygen on ring E of stachyflin, and methoxy corresponds to the hydroxy group bound to ring D. It should be noted that rings DE of stachyflin compose a large flat region and that the vanillic acid core of compound 4 mimics the flat region and the distribution of polar atoms. Diazolane of compound 4 is compatible with ring A of stachyflin, and amine on the

Table 3. Structures and Inhibitory Activities of the Synthesized Analogues to Compound 5, Which Bears a Thieno-pyrimidine Core^a



Compound	Amine	Yield (%)	EC ₅₀ (μM)
31		45	3.6
32		62	>10
33		43	>10

34		54	>10
35		28	0.6
36		82	4.6

37		48	2.0
38		32	>10
39		7	4.8

^aCondition: (b) amine, NaOH, THF, reflux, 6 h.

diazolane corresponds to the hydroxy group bound to ring A. Compound 9 in Table 2, in which diazolane is replaced by methoxy, shows a considerably high inhibitory activity. Therefore, a polar group at the position of the diazolane is not necessarily required to maintain compound potency.

Sulfur and nitrogen atoms of thieno-pyrimidine moiety of compound 5 mimic the charge distribution of rings DE. It is notable that thieno-pyrimidine also composes a large flat

region. Another thiophene and dimethylamine are compatible with rings A and B of stachyflin, respectively. The high inhibitory activity of compound 35 in Table 3 suggests that thiophene is not necessarily required to maintain compound potency. This finding provides a sound explanation for the high inhibitory activity of compound 9. Accordingly, the region of ring A of stachyflin is not so important for inhibitory activity. Instead, the flat region at rings DE and the charge distribution on the flat region are essential for compound potency.

Compound 9 and 35 were docked to the wild-type HA and the three mutants in the same manner as stachyflin was. The predicted binding structures in Supplementary Figure S8 indicate that the binding site of compound 9 changed among the models. In contrast, compound 35 was bound to almost the same location among all models. The thieno-pyrimidine moiety is positioned near D109. This position is, however, different from that of stachyflin. The sizes of compounds 9 and 35 are small compared to stachyflin and compounds 4 and 5. Hence this smallness may be a reason for the incompatibility of the binding mode. To produce potent compounds appropriately fitted to the domain between inner helices of HA, compounds 9 and 35 should be converted with retention of the vanillic acid core and/or the thieno-pyrimidine moiety and with attachment of some chemical group containing a chiral center at the opposite side to cling to the helix round surface.

METHODS

Molecular Dynamics Simulation. Information on the structural difference between the wild-type HA and the mutants is essential for clarifying the reason why some amino acid mutations in HA diminish the inhibitory activity of stachyflin. The initial structure of the wild-type HA of WSN strain was constructed by homology modeling using Modeler ver. 9.4.³⁷ The multiple-alignment technique was employed, where the X-ray crystal structures of A/Puerto Rico/8/1934 H1N1 with PDB codes 1RVZ and 1RU7³⁸ and A/Brevig Mission/1/1918 H1N1 with code 1RD8³⁹ were selected for references in modeling. Homology modeling was also performed to build the initial structures for variants; K51R and K121E mutations were introduced in the HA2 subunit in mutant 1, V176I in HA1 and K51R, K121E in HA2 in mutant 2, and V176I in HA1 and K51R in HA2 in mutant 3. A lipid bilayer of 100 Å × 100 Å was generated by using an in-house software GLYMM implemented in VMD ver. 1.8⁴⁰ for the purpose of embedding the C-terminal side of HA2 subunit into the lipid membrane mimicking the viral envelope. The composition of lipid molecules in the membrane was set to be as compatible as possible with the composition of lipid molecules in the influenza viral envelope, as shown in Supplementary Table 1. Judging from the prediction results with UniProtKB,⁴¹ amino residues 186–206 were assumed to be the transmembrane region embedded in the viral envelope. It is natural to consider that an α helix structure is formed in the transmembrane region. However, there is no experimental ground for the formation of an α helix in this region. Accordingly, this region was set to have no secondary structure, that is, to be in a strand form in the initial structure of the present simulations. In our preliminary calculation without embedding the C-terminal side of HA2 subunit into the lipid membrane, each helix in HA2 gradually changed its conformation to separate itself from other helices. HA trimer was converted from a closed shape to an open one with the progress of simulation. The motion of the C-terminal region of HA2 was large in the preliminary calculation, which seemed to be a cause of structural instability and became a trigger for the drastic conformational change. That is, the helices of the HA trimer cannot maintain the closed form unless the C-terminal side of HA2 is embedded in the lipid membrane. Hence, calculation models in this work included the membrane mimicking the viral envelope and the transmembrane region of HA. TIP3P water molecules and ions to neutralize the calculation cell were generated to solvate the complex of HA and lipid membrane, making a

periodic boundary box of $100 \text{ \AA} \times 100 \text{ \AA} \times 250 \text{ \AA}$ in which the top and bottom parts of HA were set apart from the boundary by more than 10 \AA (Figure 1c). Consequently, the total number of atoms was about 259,300 in each model.

MD simulations were carried out for every model using NAMD ver. 2.6.⁴² Initially, energy minimization was executed for 1,000,000 steps with the conjugate gradient method. Next, the temperature of the model system was elevated up to 310 K. Then 30 ns equilibrating simulation was performed in the NTP ensemble condition to obtain the equilibrated structures of the wild-type HA and the three kinds of mutants. Nonbonded interaction terms were computed with a cutoff distance of 12 \AA , where a switching distance of 10 \AA was applied to make the nonbonded interaction zero at the cutoff distance smoothly. A periodic boundary condition was applied to all directions of the calculation cell, and the particle mesh Ewald method was employed to compute the long-distance nonbonded interaction. CHARMM27 force field⁴³ was adopted for all atoms.

Docking Simulation. The binding modes of stachyflin to the wild-type HA and its mutants were predicted by docking simulation using GOLD ver. 4.^{44,45} The equilibrated structure obtained from the MD simulation was utilized as a plausible protein structure of HA in the wild-type and three mutants. Binding score was also calculated to evaluate the difference in binding affinity due to the mutations. A preliminary docking calculation was executed to search for the docking area within 30 \AA from Phe110 of the HA2 subunit. Since an adequate docking space was found inside the area and stachyflin was positioned near Asp109 in the binding mode ranking first, recalculation of stachyflin docking was performed with the search area set within 10 \AA from Asp109 of HA2 subunit. Fifty binding poses were generated and the binding affinities of those binding poses were estimated by GOLD score function. On the basis of the ranking in the estimated GOLD score, the most probable binding pose was selected. The binding affinity for the selected binding pose was re-estimated using ASP score function. This two-step approach, *i.e.*, determination of the binding pose with GOLD score and subsequent estimation of binding affinity with ASP score, was reported to successfully provide reliable prediction in docking of low-molecular-weight ligands to an enzyme or receptor.^{46,47}

In Silico Screening. A search for compounds bearing chemical features similar to those of stachyflin was made by an *in silico* pharmacophore screening. A chemical database was provided by Namiki Co. Ltd., in which about 3 million synthesized compounds are listed and all of the compounds are available by purchase. First, conformations of every compound were generated by using OMEGA module of OpenEye software.⁴⁸ Totally, more than 200 million chemical conformations were generated. Second, the pharmacophore of stachyflin was extracted for setting queries, in which hydrogen-bond donor and acceptor, aromatic ring, and hydrophobic region appeared to be key features. Third, chemical screening was carried out from the viewpoint of structural similarity to stachyflin using ROCS module of OpenEye.⁴⁹ A total of 5094 compounds were extracted from the Namiki database under the condition of the Tanimoto coefficient being more than 0.75. Fourth, more condensed selection of chemicals from the 5094 compounds was performed using EON module⁴⁹ from the viewpoint of similarity in charge distribution. The compounds without structural flexibility were excluded. Consequently, 8 chemical compounds were selected as candidates for purchase.

Synthesis of Analogue Compounds. Two series of derivatives were synthesized in this work. One is an analogue containing a vanillic acid skeleton, and the other is one bearing thieno-pyrimidine. Compound 9, 3-methoxy-4-[(methyl-sulfonyl)oxy]-benzoic acid methoxy-ester, is a typical derivative of the former series. A mixture of vanillic acid methyl (1.0 g, 5.49 mmol), KCO_3 (1.13 g, 8.24 mmol), and acetonitrile (30 mL) was cooled in an ice bath under Ar atmosphere. Methane-sulfonyl chloride (0.51 mL, 6.59 mmol) was slowly added to the mixture, and then the solution was mechanically stirred for 3 h at RT. The reaction mixture was filtered with Celite, and the solvent was removed *in vacuo*. The resulting product was extracted with a solution of EtOAc (30 mL) and 1 M aqueous HCl (30 mL). The aqueous layer was treated with EtOAc (20 mL) two times, and

the combined organic layer was washed with brine, dried over MgSO_4 , and concentrated *in vacuo*. The product was purified by thin-layer chromatography with hexane/EtOAc in a ratio of 3:1. The solid obtained was resuspended with a solution of hexane and EtOAc, and recrystallization produced the final compound as a white solid (1.01 g, yield 71%).

A typical derivative of the latter series is compound 35, 4-(4-methyl-1-piperazinyl)-thieno[2,3-*d*]pyrimidine hydrochloride salt. 4-Chloro-thieno[2,3-*d*]pyrimidine (200 mg, 1.17 mmol) was solvated with THF (15 mL). After addition of 1-methyl-piperazine (0.26 mL, 2.34 mmol) and NaOH (0.94 g, 2.34 mmol), the mixture was heated under reflux for 6 h. The solvent was removed *in vacuo*, and the reaction mixture was treated with a solution of EtOAc (20 mL) and distilled H_2O (15 mL). The product was extracted with EtOAc two times, and the organic layer was washed with brine and dried over Na_2SO_4 . The solvent was evaporated *in vacuo*, and the resulting product was purified by two-dimensional thin-layer chromatography with hexane/EtOAc in ratios of 3:1 and 1:1. A brown solid of (phenyl piperazinyl)-thienopyrimidine was obtained in a yield of 54% (148 mg). The solid obtained was resuspended in a solution of toluene (20 mL) and 1 M aqueous HCl (0.6 mL) and heated under reflux for 1 h. The reaction solution was cooled to RT, and filtration gave the final compound as a brownish solid (127 mg, yield 45%).

Antiviral Assay. Compound potency was tested by an influenza virus cell culture assay with measurement of the quantity of viral RNA using real-time polymerase chain reaction (RT-PCR). Test compounds were mixed with minimum essential medium (MEM) containing bovine serum albumin (BSA). To prepare a virus-containing compound-mixed medium, 100 units of 50% tissue culture infective dose (TCID₅₀) of influenza virus A/Perto Rico/8/34 strain (PR8) was suspended in 100 μL of the MEM-BSA containing test compounds and 10 $\mu\text{g}/\text{mL}$ of acetylated trypsin. Madin-Darby canine kidney (MDCK) cells were loaded in a 96-well plate. The cells were washed with phosphate-buffered saline (PBS), followed by 0.5–1 h incubation with compound-mixed medium. The virus-containing compound-mixed medium was also incubated for 0.5–1 h. After incubation, MDCK cells in the compound-mixed medium without viruses were transferred to the compound-mixed medium with viruses. Then the cells were incubated for 1 h at $37 \text{ }^\circ\text{C}$ in 100 μL of the virus-containing compound-mixed medium (100 TCID₅₀ influenza virus, 10 $\mu\text{g}/\text{mL}$ acetylated trypsin, and test compound at several concentrations). MDCK cells were washed with compound-mixed medium without viruses and incubated in the compound-mixed, acetylated trypsin-containing medium without influenza virus for 24 h. Culture supernatants of MDCK cells were collected after the incubation, and RNA was extracted from the supernatants. The amount of viral RNA was measured by the RT-PCR method. The measurement was compared to that of the control that was performed in a similar manner without any test compound. The compound concentration to suppress viral proliferation to 50% (EC_{50}) was estimated from the comparison.

RNA Extraction and RT-PCR. To monitor the efficiency of RNA purification, uninfected VeroE6 cells were mixed in the ISOGEN reagent as a source of 18S rRNA for normalization. Supernatants from MDCK cell culture medium were mixed with ISOGEN reagent and RNA was purified according to the manufacturer's protocol. For quantification of PR8 HA RNA, real-time RT-PCR was performed using the primers and the probe with the sequences of PR8-HA-F: 5'-GGCAAATGGAAATCTAATAGCACC-3', PR8-HA-R: 5'-TGATGCTTTTGAGGTGATGA-3', and PR8-HA-probe: 5'-FAM-TCGCACTGAGTAGAGGCTTTGGTCC-TAMRA-3'. For monitoring efficiency of RNA purification, 18S rRNA was quantified using the primers and the probe with the sequences of 18S-F: 5'-GTAACCCGTTGAACCCATT-3', 18S-R: 5'-CCATCCAATCGGTAGTAGCG-3', and 18S-probe: 5'-FAM-TGCGTGTGATTAAGTCCCTGCCCTTTGTA-TAMRA-3'. The intensity of fluorescence emitted from the probe was detected by the ABI-7700 sequence detector system (Applied Biosystems).

■ ASSOCIATED CONTENT

● Supporting Information

Composition of lipid membrane models, predicted binding affinities, RMSDs during MD simulation, predicted binding structures of stachyflin, superimposition of HA structures, chemical properties of synthesized compounds, and their NMR spectra. This material is available free of charge via the Internet at <http://pubs.acs.org>.

■ AUTHOR INFORMATION

Corresponding Author

*E-mail: (N.Y.) n-yama-5@nih.go.jp; (T.H.) hoshino@chiba-u.jp.

Author Contributions

#These authors contributed equally to this work.

■ ACKNOWLEDGMENTS

We thank L.Q. Mai (National Institute of Hygiene and Epidemiology, Hanoi) for providing the A/Vietnam/1194/04 virus strain. This work was partly supported by a Health and Labor Science Research Grant for Research from the Ministry of Health and Labor of Japan. This work was also supported by a Grant-in-Aid for Scientific Research (C) from Japan Society for the Promotion of Science (JSPS). This study was also supported in part by a grant-in-aid (S0991013) from the Ministry of Education, Culture, Sport, Science, and Technology, Japan (MEXT) for the Foundation of Strategic Research Projects in Private Universities. Theoretical calculations were performed at the Research Center for Computational Science, Okazaki, Japan and at the Information Technology Center of the University of Tokyo and also by the high-performance computer system at Institute for Media Information Technology in Chiba University.

■ REFERENCES

- (1) Gambotto, A.; Barratt-Boyes, S. M.; de Jong, M. D.; Neumann, G.; and Kawaoka, Y. (2008) Human infection with highly pathogenic H5N1 influenza virus. *Lancet* 371, 1464–1475.
- (2) Beigel, J. H.; Farrar, J.; Han, A. M.; Hayden, F. G.; Hyer, R.; de Jong, M. D.; Lochindarat, S.; Nguyen, T. K. T.; Nguyen, T. H.; Tran, T. H.; Nicoll, A.; Touch, S.; Yuen, K. Y.; and Writing Committee of the World Health Organization Consultation on Human Influenza A/H5. (2005) Avian influenza A (H5N1) infection in humans. *N. Engl. J. Med.* 353, 1374–1385.
- (3) Schnell, J. R., and Chou, J. J. (2008) Structure and mechanism of the M2 proton channel of influenza A virus. *Nature* 451, 591–595.
- (4) Stouffer, A. L.; Acharya, R.; Salom, D.; Levine, A. S.; Di Costanzo, L.; Soto, C. S.; Tereshko, V.; Nanda, V.; Stayrook, S.; and DeGrado, W. F. (2008) Structural basis for the function and inhibition of an influenza virus proton channel. *Nature* 451, 596–599.
- (5) McNicholl, I. R., and McNicholl, J. J. (2001) Neuraminidase inhibitors: zanamivir and oseltamivir. *Ann. Pharmacother.* 35, 57–70.
- (6) Moscona, A. (2005) Neuraminidase inhibitors for influenza. *N. Engl. J. Med.* 353, 1363–1373.
- (7) Bright, R. A.; Medina, M.-j.; Xu, X.; Perez-Orozco, G.; Wallis, T. R.; Davis, X. M.; Povinelli, L.; Cox, N. J.; and Klimov, A. I. (2005) Incidence of adamantane resistance among influenza A (H3N2) viruses isolated worldwide from 1994 to 2005: a cause for concern. *Lancet* 366, 1175–1181.
- (8) Deyde, V. M.; Xu, X.; Bright, R. A.; Shaw, M.; Smith, C. B.; Zhang, Y.; Shu, Y.; Gubareva, L. V.; Cox, N. J.; and Klimov, A. I. (2007) Surveillance of resistance to adamantanes among influenza A(H3N2) and A(H1N1) viruses isolated worldwide. *J. Infect. Dis.* 196, 249–257.
- (9) Kitahori, Y.; Imanishi, Y.; and Inoue, Y. (2008) High incidence of amantadine-resistant influenza H1N1 viruses isolated during the 2007–2008 season in Nara Prefecture, Japan. *Jpn. J. Infect. Dis.* 61, 253–254.
- (10) Kamigauchi, T.; Fujiwara, T.; Tani, H.; Kawamura, Y.; Horibe, I. Shionogi & Co, Ltd. Sesquiterpene derivatives having antiviral activity, Patent WO/1997/011947, 1997.
- (11) Taishi, T., Takechi, S., and Mori, S. (1998) First total synthesis of (\pm)-stachyflin. *Tetrahedron Lett.* 39, 4347–4350.
- (12) Yoshimoto, J.; Kakui, M.; Iwasaki, H.; Fujiwara, T.; Sugimoto, H.; and Hattori, N. (1999) Identification of a novel HA conformational change inhibitor of human influenza virus. *Arch. Virol.* 144, 865–878.
- (13) Yoshimoto, J.; Kakui, M.; Iwasaki, H.; Sugimoto, H.; Fujiwara, T.; and Hattori, N. (2000) Identification of amino acids of influenza virus HA responsible for resistance to a fusion inhibitor, Stachyflin. *Microbiol. Immunol.* 44, 677–685.
- (14) Rosenbaum, D. M.; Cherezov, V.; Hanson, M. A.; Rasmussen, S. G. F.; Thian, F. S.; Kobilka, T. S.; Choi, H. J.; Yao, H. J.; Weis, W. L.; Stevens, R. C.; and Kobilka, B. K. (2007) GPCR engineering yields high-resolution structural insights into β 2-adrenergic receptor function. *Science* 318, 1266–1273.
- (15) Wegener, A. A.; Klare, J. P.; Engelhard, M.; and Steinhoff, H. J. (2001) Structural insights into the early steps of receptor-transducer signal transfer in archaean phototaxis. *EMBO J.* 20, 5312–5319.
- (16) Sato, Y.; Hata, M.; Neya, S.; and Hoshino, T. (2005) Computational analysis of the transient movement of helices in sensory rhodopsin II. *Protein Sci.* 14, 183–192.
- (17) Cross, K. J.; Burleigh, L. M.; and Steinhauer, D. A. (2001) Mechanisms of cell entry by influenza virus. *Exp. Rev. Mol. Med.* 3, 1–15.
- (18) Bodian, D. L.; Yamasaki, R. B.; Buswell, R. L.; Stearns, J. F.; White, J. M.; and Kuntz, I. D. (1993) Inhibition of the fusion-inducing conformational change of influenza hemagglutinin by benzoquinones and hydroquinones. *Biochemistry* 32, 2967–2978.
- (19) Luo, G.; Colonno, R.; and Krystal, M. (1996) Characterization of hemagglutinin-specific inhibitor of influenza A virus. *Virology* 226, 66–76.
- (20) Plotch, S. J.; O'Hara, B.; Morin, J.; Palant, O.; LaRocque, J.; Bloom, J. D.; Lang, S. A. Jr.; DiGrandi, M. J.; Bradley, M.; Nilakantan, R.; and Gluzman, Y. (1999) Inhibition of influenza A virus replication by compounds interfering with the fusogenic function of the viral hemagglutinin. *J. Virol.* 73, 140–151.
- (21) Staschke, K. A.; Hatch, S. D.; Tang, J. C.; Hornback, W. J.; Munroe, J. E.; Colacino, J. M.; and Muesing, M. A. (1998) Inhibition of influenza virus hemagglutinin-mediated membrane fusion by a compound related to podocarpic acid. *Virology* 248, 264–274.
- (22) Hoffman, L. R.; Kuntz, I. D.; and White, J. M. (1997) Structure-based identification of an inducer of the low-pH conformational change in the influenza virus hemagglutinin: Irreversible inhibition of infectivity. *J. Virol.* 71, 8808–8820.
- (23) Matsubara, T.; Onishi, A.; Saito, T.; Shimada, A.; Inoue, H.; Taki, T.; Nagata, K.; Okahata, Y.; and Sato, T. (2010) Sialic acid-mimic peptides as hemagglutinin inhibitors for anti-influenza therapy. *J. Med. Chem.* 53, 4441–4449.
- (24) Feng, F.; Miura, N.; Isoda, N.; Sakoda, Y.; Okamoto, M.; Kida, H.; and Nishimura, S. (2010) Novel trivalent anti-influenza reagent. *Bioorg. Med. Chem. Lett.* 20, 3772–3776.
- (25) Tang, G.; Lin, X.; Qiu, Z.; Li, W.; Zhu, L.; Wang, L.; Li, S.; Li, H.; Lin, W.; Yang, M.; Guo, T.; Chen, L.; Lee, D.; Wu, J. Z.; and Yang, W. (2011) Design and synthesis of benzenesulfonamide derivatives as potent anti-influenza hemagglutinin inhibitors. *ACS Med. Chem. Lett.* 2, 603–607.
- (26) Sawada, T.; Fedorov, D. G.; and Kitaura, K. (2010) Role of the key mutation in the selective binding of avian and human influenza hemagglutinin to sialosides revealed by quantum-mechanical calculations. *J. Am. Chem. Soc.* 132, 16862–16872.
- (27) Takematsu, K.; Fukuzawa, K.; Omagari, K.; Nakajima, S.; Nakajima, K.; Mochizuki, Y.; Nakano, T.; Watanabe, H.; and Tanaka, S. (2009) Possibility of mutation prediction of influenza hemagglutinin

by combination of hemadsorption experiment and quantum chemical calculation for antibody binding. *J. Phys. Chem. B* 113, 4991–4994.

(28) Newhouse, E. I., Xu, D., Markwick, P. R., Amaro, R. E., Pao, H. C., Wu, K. J., Alam, M., McCammon, J. A., and Li, W. W. (2009) Mechanism of glycan receptor recognition and specificity switch for avian, swine, and human adapted influenza virus hemagglutinins: a molecular dynamics perspective. *J. Am. Chem. Soc.* 131, 17430–17442.

(29) Kasson, P. M., Ensign, D. L., and Pande, V. S. (2009) Combining molecular dynamics with bayesian analysis to predict and evaluate ligand-binding mutations in influenza hemagglutinin. *J. Am. Chem. Soc.* 131, 11338–11340.

(30) Das, P., Li, J., Royyuru, A. K., and Zhou, R. (2009) Free energy simulations reveal a double mutant avian H5N1 virus hemagglutinin with altered receptor binding specificity. *J. Comput. Chem.* 30, 1654–1663.

(31) Xu, D., Newhouse, E. I., Amaro, R. E., Pao, H. C., Cheng, L. S., Markwick, P. R., McCammon, J. A., Li, W. W., and Arzberger, P. W. (2009) Distinct glycan topology for avian and human sialopentaccharide receptor analogues upon binding different hemagglutinins: a molecular dynamics perspective. *J. Mol. Biol.* 387, 465–491.

(32) Fleishman, S. J., Whitehead, T. A., Ekiert, D. C., Dreyfus, C., Corn, J. E., Strauch, E. M., Wilson, I. A., and Baker, D. (2011) Computational design of proteins targeting the conserved stem region of influenza hemagglutinin. *Science* 332, 816–821.

(33) Watanabe, K., Sakurai, J., Abe, H., and Katoh, T. (2010) Total synthesis of (+)-stachyflin: a potential anti-influenza A virus agent. *Chem. Commun.* 46, 4055–4057.

(34) Nakatani, M., Nakamura, M., Suzuki, A., Inoue, M., and Katoh, T. (2002) A new strategy toward the total synthesis of stachyflin, a potent anti-influenza A virus agent: concise route to the tetracyclic core structure. *Org. Lett.* 4, 4483–4486.

(35) Carey, J. S., Laffan, D., Thomson, C., and Williams, M. T. (2006) Analysis of the reactions used for the preparation of drug candidate molecules. *Org. Biomol. Chem.* 4, 2337–2347.

(36) Mizukami, T., Imai, J., Hamaguchi, I., Kawamura, M., Momose, H., Naito, S., Maeyama, J., Masumi, A., Kuramitsu, M., Takizawa, K., Nomura, N., Watanabe, S., and Yamaguchi, K. (2008) Application of DNA microarray technology to influenza A/Vietnam/1194/2004 (H5N1) vaccine safety evaluation. *Vaccine* 26, 2270–2283.

(37) Sali, A., and Blundell, T. L. (1993) Comparative protein modelling by satisfaction of spatial restraints. *J. Mol. Biol.* 234, 779–815.

(38) Gamblin, S. J., Haire, L. F., Russell, R. J., Stevens, D. J., Xiao, B., Ha, Y., Vasisht, N., Steinhauer, D. A., Daniels, R. S., Elliot, A., Wiley, D. C., and Skehel, J. J. (2004) The structure and receptor binding properties of the 1918 influenza hemagglutinin. *Science* 303, 1838–1842.

(39) Stevens, J., Corper, A. L., Basler, C. F., Taubenberger, J. K., Palese, P., and Wilson, I. A. (2004) Structure of the uncleaved human H1 hemagglutinin from the extinct 1918 influenza virus. *Science* 303, 1866–1870.

(40) Humphrey, W., Dalke, A., and Schulten, K. (1996) VMD: visual molecular dynamics. *J. Mol. Graph.* 14, 33–38.

(41) The UniProt Consortium. (2011) Ongoing and future developments at the Universal Protein Resource. *Nucleic Acids Res.* 39, D214–D219.

(42) Phillips, J. C., Braun, R., Wang, W., Gumbart, J., Tajkhorshid, E., Villa, E., Chipot, C., Skeel, R. D., Kalé, L., and Schulten, K. (2005) Scalable molecular dynamics with NAMD. *J. Comput. Chem.* 26, 1781–1802.

(43) Feller, S. E., Gawrisch, K., and MacKerell, A. D. (2002) Polyunsaturated fatty acids in lipid bilayers: intrinsic and environmental contributions to their unique physical properties. *J. Am. Chem. Soc.* 124, 318–326.

(44) Jones, G., Willett, P., Glen, R. C., Leach, A. R., and Taylor, R. (1997) Development and validation of a genetic algorithm for flexible docking. *J. Mol. Biol.* 267, 727–748.

(45) Jones, G., Willett, P., and Glen, R. C. (1995) Molecular recognition of receptor sites using a genetic algorithm with a description of desolvation. *J. Mol. Biol.* 245, 43–53.

(46) Verdonk, M. L., Cole, J. C., Hartshorn, M. J., Murray, C. W., and Taylor, R. D. (2003) Improved protein-ligand docking using GOLD. *Proteins: Struct., Funct., Genet.* 52, 609–623.

(47) Mooij, W. T. M., and Verdonk, M. L. (2005) General and targeted statistical potentials for protein-ligand interactions. *Proteins: Struct., Funct., Genet.* 61, 272–281.

(48) Bostrom, J., Greenwood, J. R., and Gottfries, J. (2003) Assessing the performance of OMEGA with respect to retrieving bioactive conformations. *J. Mol. Graphics Modell.* 21, 449–462.

(49) OpenEye Scientific Software, Inc., Santa Fe, NM, USA, www.eyesopen.com.

Structural Modulation Study of Inhibitory Compounds for Ribonuclease H Activity of Human Immunodeficiency Virus Type 1 Reverse Transcriptase

Hiroshi Yanagita,^a Satoshi Fudo,^a Emiko Urano,^b Reiko Ichikawa,^b Masakazu Ogata,^a Mizuho Yokota,^a Tsutomu Murakami,^b Honggui Wu,^{b,c} Joe Chiba,^c Jun Komano,^b and Tyuji Hoshino^{*a}

^a Graduate School of Pharmaceutical Sciences, Chiba University; 1–8–1 Inohana, Chuo-ku, Chiba 260–8675, Japan:

^b AIDS Research Center, National Institute of Infectious Diseases; 1–23–1 Toyama, Shinjuku-ku, Tokyo 162–8640,

Japan; and ^c Faculty of Industrial Science and Technology, Tokyo University of Science; 2641 Yamazaki, Noda, Chiba 278–8510, Japan. Received February 23, 2012; accepted April 4, 2012

Reverse transcriptase of human immunodeficiency virus type 1 (HIV-1) has two enzymatic functions. One of the functions is ribonuclease (RNase) H activity concerning the digestion of only RNA of RNA/DNA hybrid. The RNase H activity is an attractive target for a new class of anti-HIV drugs because no approved inhibitor is available now. In our previous studies, an agent bearing 5-nitro-furan-2-carboxylic acid ester core was found from chemical screening and dozens of the derivatives were synthesized to improve compound potency. In this work, some parts of the chemical structure were modulated to deepen our understanding of the structure–activity relationship of the analogous compounds. Several derivatives having nitro-furan-phenyl-ester skeleton were shown to be potent RNase H inhibitors. Attaching methoxy-carbonyl and methoxy groups to the phenyl ring increased the inhibitory potency. No significant cytotoxicity was observed for these active derivatives. In contrast, the derivatives having nitro-furan-benzyl-ester skeleton showed modest inhibitory activities regardless of attaching diverse kinds of functional groups to the benzyl ring. Both the modulation of the 5-nitro-furan-2-carboxylic moiety and the conversion of the ester linkage resulted in a drastic decrease in inhibitory potency. These findings are informative for designing potent inhibitors of RNase H enzymatic activity of HIV-1.

Key words antiviral drug; human immunodeficiency virus type 1 reverse transcriptase; ribonuclease H enzymatic activity; inhibitor; nitro-furan-phenyl-ester

Human immunodeficiency virus type 1 (HIV-1) reverse transcriptase (RT) is a multi-functional enzyme that facilitates both polymerase and ribonuclease (RNase) H activities and converts the single-stranded viral RNA into a double-stranded DNA. There exist two active sites in HIV-1 RT responsible for the respective enzymatic functions. Currently, two classes of RT inhibitors, nucleoside reverse transcriptase inhibitors (NRTIs) and non-nucleoside reverse transcriptase inhibitors (NNRTIs), are used clinically. The formers compete with the natural deoxyribonucleotide triphosphate (dNTP) for nucleoside incorporation and act as chain terminators after incorporation.¹⁾ The latter agents are bound to an adjacent location from the polymerase active site and block RT polymerase function.²⁾ Both of these inhibitors are targeting polymerase activity of RT. In contrast, no approved inhibitor is available for RNase H activity, although there have been several reports on the inhibitors that target the RNase H activity of HIV-1 RT.^{3–5)} The role of RNase H activity in the reverse transcription process is to remove the viral genomic RNA during the synthesis of double-stranded DNA.^{6,7)} Agents targeting RNase H function is expected to be complementary to the currently standard chemotherapy. Hence, RT-associated RNase H activity is one of the attractive targets for developing a novel class of antiviral drugs. Furthermore, the potential for dual inhibition of RNase H activity and integrase activity of HIV-1 has been examined because of the structural similarity of their catalytic sites.^{8–10)}

HIV-1 RNase H is known to utilize two divalent metals for

catalysis.^{11–13)} The RNase H dual metal mechanism was suggested from high resolution co-crystal structures of *B. halodurans* RNase H with RNA/DNA hybrids at different stages along the reaction pathway of phosphodiester cleavage.^{14,15)} The active site contains four carboxyl residues, creating an environment capable of holding two metal ions. It has been assumed that many RNase H inhibitors bind to the catalytic center interacting with two divalent metal ions simultaneously. Diketo acids are known to work as potent inhibitors for divalent metal-related enzymes.¹⁶⁾ Therefore, diketo acid structure has served as a starting point for the design and optimization of inhibitors of HIV-1 integrase or influenza endonuclease. Pyrimidinol is another typical agent bearing a scaffold called *N*-hydroxyimide.¹⁷⁾ *N*-Hydroxyimides were firstly described as inhibitors of influenza endonuclease, but they also show a high potency in biochemical assays of HIV-1 RNase H. A natural product β -thujaplicinol is another scaffold and shows a high inhibitory potency for HIV-1 RNase H activity.¹⁸⁾

From an *in vitro* screening using 20000 chemical compounds, we found chemicals that blocked HIV-1 RT-associated RNase H activity.¹⁹⁾ The agents bearing the 5-nitro-furan-2-carboxylic acid ester moiety turned out to work as an RNase H inhibitor. Two of the agents were capable of suppressing HIV-1 replication in tissue culture. On the basis of the hit chemicals found in the screening, more than 50 derivatives of 5-nitro-furan-2-carboxylic acid were synthesized.²⁰⁾ Inhibitory potency of RNase H enzymatic activity was measured in a biochemical assay. Several derivatives showed higher inhibitory activities than those of the hit chemicals. Modulation of

The authors declare no conflict of interest.

* To whom correspondence should be addressed. e-mail: hoshino@chiba-u.jp

the 5-nitro-furan-2-carboxylic moiety resulted in a decrease in inhibitory potency. In contrast, many derivatives with modulation of other parts maintained inhibitory activities. These studies indicate that the nitro-furan-carboxylic moiety is one of the potent scaffolds for RNase H inhibitor.

In this study, we further synthesized chemical compounds bearing the 5-nitro-furan-2-carboxylic acid ester moiety and examined the potency for anti-HIV drugs blocking RT-associated RNase H enzymatic activity. The potency of the synthesized compounds was evaluated through the measurement of inhibitory activity with real-time monitoring of fluorescence emission from the digested RNA substrate. In addition, the cytotoxicity of these compounds was assessed in 293T cells. Computer simulation with molecular dynamics (MD) method was also performed to analyze the stability of the binding structure of an active compound.

Experimental

Organic Synthesis Compound **1** was synthesized by creating an ester linkage between a nitro-furan carboxylic acid and an α -chloro-amide bound with benzyl and penthyl groups, by 3 h reaction at 60°C in dimethylformamide (DMF) in the presence of dimethyl-aminopyridine (DMAP). Chemical modulation was performed for the nitro-furan moiety, with changing the starting block from furan to thiophene or pyrrole *etc.* **2–8**. These compounds **2–8** were synthesized in the similar manner to compound **1**. The derivatives bearing 5-nitro-furan-2-ester scaffold, compounds **9–27**, were prepared by the reaction of converting 5-nitro-2-furoic acid into an acid chloride with thionyl chloride, followed by the nucleophilic substitution reaction in the presence of NEt_3 in tetrahydrofuran (THF) with setting the temperature at 0°C for the initial 30 min. and elevated it to r.t. afterward. Since a hydroxy group bound to phenyl ring is more reactive than a hydroxy group bound to alkane, the substitution reaction dominantly produced phenyl-ester linkage (**9–16**) when a nucleophilic reagent contained two hydroxy groups. When a nucleophilic reagent contained only one hydroxy group, the substitution reaction generated alkyl-ester linkage (**17–27**). Compounds **28–30** were produced by generating nitro-furan-carbonyl-alkyl-benzene through the reaction of Weinreb amides containing benzyl group with alkyl lithium, followed by incorporation of nitro group into the phenyl ring using white fuming nitric acid and acetic anhydride. Compounds **29** and **30** were separated by flash chromatography. Compounds **31–33** were generated by using hydroxy-amines as nucleophilic reagents.

Evaluation of Inhibitory Activity The 50% inhibitory concentration (IC_{50}) of the synthesized compounds for RT-associated RNase H activity was determined from the chemical concentration reducing the rate for substrate cleavage reaction to half relative to the control. A real-time monitoring assay was employed to estimate the IC_{50} .^{21,22} In short, two oligo-nucleotides were annealed at final concentrations of 2.5 and 0.25 μM for substrate. One was oligo-ribonucleotide 5'-GAUCUGAGCCUGGGAGCU-3' with 6-carboxy-fluorescein (FAM) conjugated at the 3' end, and the other was oligo-deoxyribonucleotide 5'-AGCTCCCAGGCTCAGATC-3' with black hole quencher (BHQ) conjugated at the 5' end. Enzyme reaction with 100 ng RT, 0.025 μM oligo-ribonucleotide, and 0.25 μM oligo-deoxyribonucleotide was carried out in a volume of 10 μL at 37°C. Fluorescence at 488 nm was monitored every

150 s using a multimode detector.

HIV-1 RT was expressed in *E. coli* and purified by using a HiTrap Ni affinity column. The purified RT was dialyzed to reduce the concentration of imidazole from the elution buffer and then incubated with human rino virus (HRV) 3C protease to cleave an N-terminal hexahistidine tag. The protein was further purified by nickel-coordinated nitrilotriacetic acid (Ni-NTA) to remove the uncleaved protein and HRV 3C protease. The RT was dialyzed against a buffer of 50 mM Tris-HCl at pH 7.5 and 200 mM NaCl and was stored at -20°C with adding 50% (v/v) glycerol.

Assessment of Cytotoxicity 3-(4,5-Dimethylthiazol-2-yl)-2,5-diphenyltetrazolium bromide (MTT) assay was carried out with 293T cell line. First, 100 μL medium (RPMI-1640) supplemented with 10% fetal bovine serum (FBS) containing 2% dimethylsulfoxide (DMSO) was loaded in a 96-well plate, and 200 μL medium with 10% FBS and 2% DMSO containing test compounds at a concentration of 200 μM was added to the wells in the first column of the plate. Different concentrations of compound were prepared for the second, third and fourth columns. The final concentrations of these columns were 100, 50, 25 and 12.5 μM , respectively. Second, 100 μL 293T cells at a concentration of $2 \times 10^5/\text{mL}$ were added to the respective wells. The final concentration of DMSO in each well was 1%. Third, cells were incubated for 3 d at 37°C with 5% CO_2 atmosphere. A hundred micro liter of supernatant was removed from the cultured medium and 15 μL MTT reagent for dye solution was added to each well and the cells were incubated for 1 h. Then, 100 μL solution of stop mix was added, and the cells were incubated overnight at 4°C to sufficiently dissolve the dye. Finally, intensity of $\text{OD}_{570/690}$ was measured by a spectrofluorometer.

Molecular Dynamics Simulation A computational model of HIV-1 RT domain was constructed from an X-ray crystal structure with Protein Data Bank code 3QIO.²³ Atom coordinates for the missing residues were generated by using Modeller9.9.²⁴ According to the results of the recent X-ray crystallographic studies on the complex of RNase H domain and its inhibitors,^{25–27} the RNase H domain contains two divalent metal ions at the center of the active site. Two Mn^{2+} ions in the crystal structure were replaced with Mg^{2+} ions. The protonation states of all of the ionizable residues were predicted by PropKa program²⁸ in the presence of two Mg^{2+} ions at the active site. Atom charges of the compounds were determined from the electrostatic potential obtained from quantum chemical calculations, followed by the restrained electrostatic potential (RESP) fitting²⁹ in a similar manner to the previous studies.^{30–33} The atom charge for Mg^{2+} ion was setting to 1.54, which was also determined by the RESP method based on the calculated electrostatic potential obtained by QM/MM technique carried out in a similar manner to the previous work.²⁰ An active compound was combined with HIV-1 RT domain, referring the binding structure predicted in our previous work.²⁰ The compound-bound RT model was placed in a rectangular box and solvated with TIP3P water molecules,³⁴ with all of the crystal water molecules remaining. Periodic boundary conditions were applied to avoid the edge effect in all calculations.

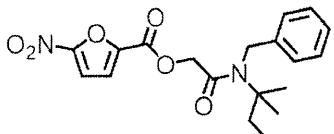
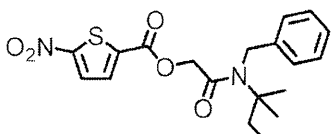
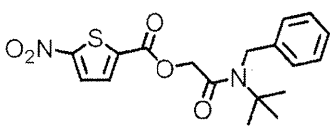
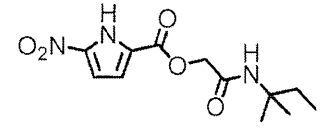
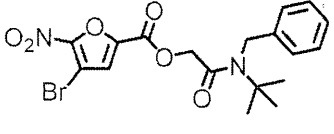
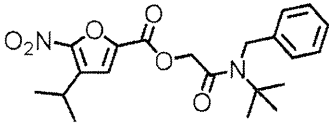
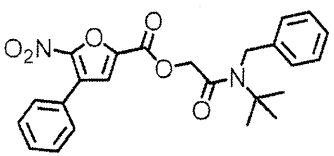
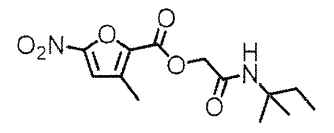
Minimizations and MD simulations were carried out using sander module of AMBER9.³⁵ The modified ff03 force field³⁶ was used as the parameters for molecular dynamics.

The cutoff distance for the long range electrostatic and van der Waals energy terms was set to 12.0 Å. The expansion and shrinkage of all covalent bonds connecting to hydrogen atom were constrained using the SHAKE algorithm.³⁷⁾ Energy minimization was achieved in three steps. Initially, movement was allowed only for water molecules. Next, compound and divalent metal ions were allowed to move in addition to the water molecules. Finally, all atoms were allowed to move freely. In each step, energy minimization was executed by the steepest descent method for the first 10000 cycles and the conjugated gradient method for the subsequent 10000 cycles. After a 0.1 ns heating calculation until 310K using the NVT ensemble condition, a 20 ns equilibrating calculation was executed at 1.0 atm and at 310K under the NPT ensemble condition, with an integration time step of 2.0 fs.

Results

Eight analogues of 5-nitro-furan-2-carboxylic acid ester were synthesized by converting the 5-nitro-furan moiety into other functional groups and examined for their RNase H inhibitory activities (Table 1). Compound **1** has a typical chemical structure showing an inhibitory potency for HIV-1 RNase H enzymatic activity. This compound bears nitro-furan ester core connecting to the pentyl- and benzyl-bound amide group. Replacement of furan with thiophene largely decreased compound potency (**2**, **3**). Conversion of furan into pyrrole also resulted in complete loss of compound potency (**4**). Attaching a halogen to the 4th position of furan exhibited a slight increase of inhibitory activity (**5**), while a hydrophobic or aromatic substitute resulted in loss of inhibitory potency (**6**, **7**). Introduction of even a small hydrophobic group at the 3rd position of furan decreased inhibitory activity (**8**).

Table 1. RNase H Inhibitory Activity and Cytotoxicity of the Derivatives Modulated at Nitro-Furan Moiety

Compound	Structure	IC ₅₀ (μM)	CC ₅₀ (μM)
1		8.4	74
2		>50	49
3		30.3	50
4		>50	86
5		6.6	3
6		>50	>100
7		>50	>100
8		25.7	76